

1 **Morphometry of tidal meander cutoffs indicates similarity to fluvial morphodynamics**

2 **C. Gao^{1,2}, E.D. Lazarus³, A. D’Alpaos², M. Ghinassi², A. Ielpi⁴, G. Parker^{5,6}, A. Rinaldo^{7,8}, P.**
3 **Gao⁹, Y.P. Wang^{1,10}, D. Tognin⁷, and A. Finotello^{2,*}**

4 *¹ Ministry of Education Key Laboratory for Coast and Island Development, School of Geographic*
5 *and Oceanographic Sciences, Nanjing University, Nanjing, China.*

6 *² Dept. of Geosciences, University of Padova, Padova, Italy.*

7 *³ School of Geography & Environmental Science, University of Southampton, Southampton, UK.*

8 *⁴ Department of Earth, Environmental and Geographic Sciences, University of British Columbia-*
9 *Okanagan, Kelowna, BC, Canada.*

10 *⁵ Department of Civil & Environmental Engineering, University of Illinois, Urbana, IL, USA*

11 *⁶ Department of Geology, University of Illinois, Urbana, IL, USA*

12 *⁷ Department of Civil, Environmental, and Architectural Engineering, University of Padova,*
13 *Padova, Italy*

14 *⁸ Laboratory of Ecohydrology, Ecole Polytechnique Federale Lausanne, Lausanne, Switzerland*

15 *⁹ Department of Geography and the Environment, Syracuse University, Syracuse, NY, USA.*

16 *¹⁰ State Key Laboratory of Estuarine and Coastal Research, School of Marine Sciences, East*
17 *China Normal University, Shanghai, China*

18

19 * Corresponding author: Alvise Finotello (alvise.finotello@unipd.it)

20 **Key Points:**

- 21 • Tidal meander cutoffs are far more common than typically thought and share remarkable
22 morphometric similarities with fluvial counterparts.
- 23 • Similar mechanisms trigger cutoffs in both tidal and fluvial landscapes, with differences
24 arising only during post-cutoff evolution.
- 25 • Tidal cutoffs seldom disconnect from parent channels and rarely form oxbows due to the
26 high hydrological connectivity of tidal wetlands.
27

28 **Abstract**

29 Sinuous channels wandering through coastal wetlands have been thought to lack lateral-migration
30 features like meander cutoffs and oxbows, spurring the broad interpretation that tidal and fluvial
31 meanders differ morphodynamically. Motivated by recent work showing similarities in planform
32 dynamics between tidal and fluvial meandering channels, we analyzed meander neck cutoffs from
33 diverse tidal and fluvial environments worldwide, and show that tidal cutoffs are widespread. Their
34 perceived paucity stems from pronounced channel density and hydrological connectivity in coastal
35 wetlands, comparatively small size of most tidal channels, and typically dense vegetation cover.
36 Although these factors do not efface tidal meander cutoffs, they collectively inhibit oxbow
37 formation and make tidal cutoffs ephemeral features that can escape detection. We argue that
38 similar morphodynamic processes drive cutoff formation in tidal and fluvial landscapes, with
39 differences arising only during post-cutoff evolution. Such process similarity has important
40 implications for understanding coastal wetland ecomorphodynamics and predicting their long-
41 term evolution.

42 **Plain Language Summary**

43 The sinuous channels that wander through tidal coastal wetlands look like meandering rivers.
44 However, features of alluvial floodplains that indicate active river meandering over time, such as
45 oxbow lakes and meander cutoffs, are difficult to find in tidal settings. Their apparent absence has
46 led researchers to infer that tidal and fluvial meanders evolve differently. We re-examined this
47 inference by identifying, measuring, and compiling examples of meander cutoffs from a variety of
48 tidal coastal wetlands and fluvial floodplains worldwide. Our analysis suggests that the shapes and
49 geometric properties of tidal and fluvial cutoffs are indeed remarkably similar. This indicates that
50 while tidal and fluvial environments differ in many ways, they nevertheless share the same
51 physical mechanism affecting meander morphodynamical evolution. Differences between tidal
52 and fluvial meanders do arise after a meander is cut off. We observe that tidal meanders remain
53 preferentially connected to the parent channel, preventing the formation of crescent-shaped oxbow
54 lakes and thus making tidal cutoffs more difficult to detect. Our results indicate a close similarity
55 in meandering channel behavior across tidal and fluvial systems, which opens new opportunities
56 for how researchers model tidal wetlands, with important implications for the effective
57 conservation and restoration of these critical ecosystems.
58

59 **1 Introduction**

60 Sinuous meandering channels are common in fluvial and coastal landscapes (Leopold et al., 1964).
61 Meandering channels migrate laterally through erosion and deposition of sediment along the outer
62 and inner banks, respectively, of individual meander bends. As meanders evolve, channels
63 frequently shortcut themselves through cutoffs and form oxbow lakes (hereinafter "oxbows";
64 Dunne & Aalto, 2013; Schwenk et al., 2015; Stølum, 1996). Cutoffs, by which oxbows are formed
65 (Dieras, 2013; Thomas et al., 2022) reduce channel sinuosity, modify rates of lateral migration,
66 and affect floodplain sedimentology, stratigraphy, and sediment residence times (Camporeale et
67 al., 2005; Howard & Hemberger, 1991; Zinger et al., 2011). These dynamics have broad
68 implications for the flux, storage, and sequestration of soil organic carbon (Torres et al., 2017).
69 Meandering river floodplains feature visible evidence of meander migration such as scroll bars
70 and oxbows (Constantine & Dunne, 2008; Dunne & Aalto, 2013; Hooke, 2013) In contrast,
71 channels in tidal coastal floodplains have been thought to lack meander cutoffs, indicating an
72 absence of active meandering (Gabet, 1998; Johnson, 1929) (Figure 1). The perceived stability of
73 sinuous tidal channels – or at least the relative subtlety of their meandering dynamics – has often
74 been attributed to the unique ecomorphodynamics of coastal environments, where flow
75 bidirectionality is paramount (Fagherazzi et al., 2004; Hughes, 2012; Solari et al., 2002). However,
76 recent studies highlighted morphodynamic commonalities between fluvial and tidal meanders,
77 with similar planform dynamics, width-adjusted migration rates, and morphodynamic regimes in
78 high-amplitude bends (Finotello et al., 2018, 2022; Gao, Finotello, & Wang, 2022; Leuven et al.,
79 2016, 2018). This motivated us to question the perceived paucity of tidal meander cutoffs, and to
80 further demonstrate the parallels between tidal and fluvial meandering channels. Here, we
81 analyzed the planform geometry of 600 tidal meander cutoffs identified in high-resolution satellite
82 images from settings around the world, characterized by different tidal regimes, vegetation cover,
83 and geomorphological backgrounds. We conducted a direct comparison with 158 cutoffs in
84 meandering rivers, uncovering striking geometric parallels. These similarities, supported by
85 theoretical, numerical, and field research, suggest a fundamental commonality in morphodynamics
86 across both tidal and fluvial domains.

87 **2 Material and Methods**

88 *2.1 Data collection*

89 We used high-resolution satellite images, freely available from Google Earth Pro, to detect
90 instances of meander cutoffs undisturbed by anthropic activities. These cutoffs, selected for their
91 geographical diversity, span coastal zones and inland alluvial plains across varied climatic and
92 geological settings. Thus, the sampled cutoffs reflect a range of hydrological and tidal regimes,
93 sediment grain sizes, vegetation types, and land cover (Figure 1a-g). Our full dataset includes over
94 1200 examples of tidal cutoffs. Of these 1200 examples, 600 tidal cutoffs with clearly discernable
95 boundaries were manually digitized as polygons using Google Earth Pro. The remainder lacked
96 sufficient detail to be digitized due to poor preservation, dense vegetation canopy, low image
97 resolution, complex morphology resulting from multiple cutoffs, or combinations of these factors,
98 and were categorized as “unanalyzed cases” (Gao & Finotello, 2023). Furthermore, we obtained
99 an additional set of 158 fluvial cutoffs specifically digitized for comparative analyses. These
100 cutoffs were extracted from rivers located in various regions, including the Amazon Basin, the
101 conterminous USA and Alaska, Russia, Canada, Kazakhstan, and New Zealand. The selection was

102 made to ensure a diverse range of channel sizes, with river widths spanning approximately four
103 orders of magnitude (Figure 2).

104 Tidal cutoffs were also further classified based on several criteria: tidal regime (microtidal $n=315$;
105 mesotidal $n=249$; macrotidal $n=36$), vegetation cover (mangroves $n=118$; salt marshes $n=433$; tidal
106 flats $n=49$), and geomorphological setting (bays $n=164$; back-barrier lagoons $n=219$; open coasts
107 $n=105$; estuaries $n=112$) (Figure S1 in Supporting Information). The mean tidal range (MTR) at
108 each site was determined by analyzing tidal gauge data from Dong (2020) and the National
109 Oceanic and Atmospheric Administration (<https://tidesandcurrents.noaa.gov/>), and individual
110 study cases were classified as macro-tidal ($MTR > 4$ m), meso-tidal ($2 < MTR < 4$ m), and
111 microtidal ($MTR < 2$ m).

112 We focus only on ‘neck’ cutoffs, formed when a high-amplitude loop gets isolated by the pinching
113 connection of two adjacent bends. In the tidal settings we examined, we found no ‘chute’ cutoffs,
114 which are formed when a river bend is shortcut by a new channel cutting through meander point
115 bars – and possibly observed in large, sand-bedded, multi-thread estuarine channels (Leuven et al.,
116 2016).

117 2.2 Data analysis

118 To calculate their morphometric parameters, cutoff polygons were projected into appropriate UTM
119 coordinates and converted to binary images. The channel centerline was computed based on a
120 standard skeletonization procedure and then resampled using standard cubic spline-fit polylines.
121 Cutoff endpoints were determined as the two branchpoints of the polygon skeleton (Figure 11). To
122 further quantify cutoff planform features, we computed the curvature \mathcal{C} ($[m^{-1}]$) of the channel
123 centerline as $\mathcal{C} = -d\theta/ds$, where θ is the angle between the tangent to the channel axis and an
124 arbitrarily selected reference direction, $x(s)$ and $y(s)$ are the Cartesian coordinates of a given
125 centerline point, and s is the intrinsic (i.e., along-channel) coordinate, assumed to be positive in
126 the upstream (i.e., landward) direction. Because flow orientation within tidal meanders changes
127 with tidal phases, we hereinafter assume a river-like reference system in which the terms
128 ‘upstream’ and ‘downstream’ refer to landward and seaward directions, respectively.

129 After computing curvature, a Savitzky–Golay low-pass filter was applied to smooth noise in the
130 original signal. Then, the apex of any individual cutoff was identified as the locus of maximum
131 curvature (Figure 11), and the cutoff asymmetry index was computed as $\mathcal{A} = (\ell_u - \ell_d)/(\ell_u +$
132 $\ell_d)$ ([-]) where ℓ_u and ℓ_d are the distances between the cutoff apex and its upstream and
133 downstream endpoints, respectively (Figure 11). Negative values of \mathcal{A} correspond to upstream-
134 skewed cutoffs, and positive values of \mathcal{A} to downstream-skewed cutoffs. Other morphometric
135 parameters were also calculated, including: average channel width W ([-]); cutoff intrinsic length
136 $\ell = \ell_u + \ell_d$ ([m]); cutoff cartesian length L ([m]), which is the planar distance between cutoff
137 endpoints; cutoff sinuosity $\chi = \ell/L$ ([-]); cutoff amplitude A ([-]), computed as the maximum
138 point-line distance between the cutoff centerline and the line connecting the two cutoff endpoints;
139 cutoff radius of curvature R ([m]), defined as the radius of the best-fitting circle through all cutoff
140 axis points; and flow-diversion angle Φ between the cutoff and its parent channel (Figure 11).
141 Because of bidirectional flow through tidal channels, morphodynamically meaningful flow-
142 diversion angles can be identified at both the cutoff upstream (Φ_u) and downstream (Φ_d) ends. By
143 comparison, because of the unidirectional flow through river channels, only the upstream flow-
144 diversion angle (Φ_u) is morphodynamically meaningful for fluvial cutoffs (Dieras, 2013).

145 To directly compare meander cutoffs of different sizes, dimensional morphometric variables were
146 normalized using channel width (W), such that width-adjusted cutoff radius of curvature,
147 amplitude, and lengths are defined as $R^* = R/W$, $A^* = A/W$, $L^* = L/W$, and $\ell^* = \ell/W$.

148 3 Results

149 Dimensional morphometrics – R , A , and ℓ – all exhibit statistically significant power-law
150 relationships to cutoff width W (p -value < 0.01) with matching best-fit power-law exponents and
151 limited separation in power-law scaling constants (Figure 2 and Figure S2 in Supporting
152 Information). We also found a statistically significant quasi-linear relation between L and W
153 (Figure S3 in Supporting Information), with $L \cong W$. The latter has been described previously as
154 the condition leading to neck cutoff (Li et al., 2022), whereas $L < W$ represents a geometrically
155 impossible configuration (Hayden et al., 2021). Similarly, radius of curvature $R = W/2$ represents
156 a physically meaningful lower bound, since the edges of a channel centerline with a radius of
157 curvature smaller than half its width would intersect each other (Hayden et al., 2021). Although
158 theoretically there are no physical limits to the development of both A and ℓ (besides the basic
159 requirements that $A > 0$ and $\ell > L$ in order for a centerline to be sinuous), the prevalence of smaller
160 curves weights the distribution of meander features toward the physically meaningful lower bound
161 (Vermeulen et al., 2016). For these reasons, the scaling similarity in dimensional metrics reported
162 in Figure 2 is likely due to the finite-width nature of the sinuous features we measured, rather than
163 representing a suitable diagnostic with which to distinguish the fluvial or tidal nature of meander
164 cutoffs. Indeed, previous studies suggest that dimensionless meander morphometrics should be
165 used to infer morphological similarity (Frascati & Lanzoni, 2009; Howard & Hemberger, 1991).
166 We thus performed Kolmogorov-Smirnov (KS) tests ($\alpha = 0.05$) on dimensionless morphometric
167 descriptors to highlight that tidal cutoffs are typically less sinuous (i.e., lower χ) and feature
168 smaller with-adjusted radii (R^*), amplitudes (A^*), and intrinsic lengths (ℓ^*) (Figure 3 and Table S1
169 in Supporting Information).

170 Since meander size and sinuosity are expected to increase with time, our findings indicate that
171 tidal cutoffs are less morphodynamically mature (i.e., less sinuous and planimetrically complex)
172 than their fluvial counterparts. This points to an overall faster evolutionary trajectory from
173 meander inception to cutoffs in tidal settings. However, similar width-adjusted meander migration
174 rates in tidal and fluvial settings (Finotello et al., 2018) contrast with such an interpretation.
175 Furthermore, KS tests demonstrate similar values of asymmetry (\mathcal{A}) and upstream flow-diversion
176 angle (Φ_u) in tidal and fluvial cutoffs (Figure 3 and Table S1 in Supporting Information). Given
177 that neither of these parameters are affected by meander size, the observed similarity not only
178 reflects similar morphodynamic maturity but also suggest shared cutoff-triggering mechanisms,
179 likely associated with the planform configuration of the parent channel (Dieras, 2013). Notably,
180 both fluvial and tidal cutoffs exhibit negative median and peak values of the asymmetry index \mathcal{A}
181 (Figure 3e). That is, both types of cutoffs tend to be upstream-skewed, supporting similarity in
182 their dominant morphodynamic regime (*sensu* Seminara et al., 2001). This observation likely
183 stems from the morphodynamic dominance, in tidal channels, of either flood or (more commonly)
184 ebb flows that effectively render tidal meanders similar to their fluvial counterparts featuring
185 unidirectional flows (Fagherazzi et al., 2004; Kleinhans et al., 2009).

186 We propose that the comparatively smaller size of tidal cutoffs, relative to fluvial ones, is not a
187 result of fundamental differences in their morphodynamics. Instead, it appears to be predominantly
188 influenced by the specific hydrological, ecological, and geomorphological attributes inherent to
189 tidal wetlands. Specifically, we hypothesize that the dense distribution of tidal channels that

190 typically characterizes tidal wetlands accounts for the reduced size and sinuosity of tidal cutoffs,
191 with enhanced hydrological connectivity explaining the apparent paucity of cutoff traces in tidal
192 environments as we discuss below.

193 **4 Discussion**

194 *4.1 Dense channel distribution limits stream meandering and cutoff formation*

195 Meander migration in densely channeled tidal floodplains shapes the landscape differently than in
196 fluvial contexts, where rivers can freely migrate laterally without intercepting other channels and
197 confluences are comparatively infrequent. Tidal wetlands are characterized by high drainage
198 density – taken as the mean shortest distance that a parcel of water placed on the wetland surface
199 would need to travel before reaching the closest channel (Marani et al., 2003). Such enhanced
200 drainage density limits meander dynamics by preventing channels from freely migrating and
201 meanders from fully developing without intercepting adjoining streams (Letzsch & Frey, 1980;
202 Vilas et al., 1999). A similar dynamic is described in multi-thread, anabranching rivers with
203 individual sinuous anabranches, where enhanced channel density limits cutoff formation (Schumm
204 et al., 1996). Accordingly, evidence from modern and ancient deposits shows that channel piracy
205 (i.e., stream captures) in dense tidal networks (Figure S4 in Supporting Information) limit the
206 lateral accretion of point bar bodies and can modify the network-scale distribution of the tidal
207 prism, feeding back into the long term ecomorphodynamic evolution of the entire tidal system
208 (Cosma et al., 2020; Finotello, Ghinassi, et al., 2020). Hence, enhanced channel density limits tidal
209 meander dynamics and cutoff formation.

210 Our hypothesis is further corroborated by systematic statistically significant differences observed
211 in the distributions of R^* , A^* , L^* , and χ as a function of vegetation cover, with effects of tidal
212 regime and geomorphological background being significant but less systematic (Figure 3 and
213 Tables S2 to S13 in Supporting Information). Tidal cutoffs in salt marshes are smaller and less
214 sinuous than those found in mangrove forests and tidal flats (Figure 3).

215 This trend resonates with existing research indicating that tidal channel networks are denser in
216 vegetated areas, especially in salt marshes (Kearney & Fagherazzi, 2016; Schwarz et al., 2022).
217 This evidence supports our contention that in densely channelized tidal wetlands, meander cutoffs
218 are constrained in their size and sinuosity growth due to the increased likelihood of channel piracy
219 during lateral migration. Similar cutoff asymmetries (\mathcal{A}) and flow-diversion angles (Φ_u , Φ_d)
220 among distinct tidal settings also support similarity in the morphodynamic processes responsible
221 for cutoff development. Kolmogorov-Smirnov tests reveal significant differences in the
222 distributions of Φ_u , Φ_d , and \mathcal{A} only based on geomorphological setting (Tables S2 to S13 in
223 Supporting Information), but we find no differences in these morphometrics as a function of tidal
224 range and vegetation cover despite the potential influence that both controls can exert on channel
225 bank erosion (Gao, Finotello, D'Alpaos, et al., 2022; Gasparotto et al., 2022; Zhao et al., 2022).

226 *4.2 Hydrological connectivity control on post-cutoff development*

227 To further substantiate that differences in tidal and fluvial cutoff morphology do not stem from
228 dissimilarities in meander morphodynamics, we also examined the connection state of individual
229 cutoffs with their parent channels. Once a river meander is cut off, a plug bar forms in response to
230 flow separation and reduced energy conditions, leading to the rapid deposition of coarse sediment
231 and blockage of both cutoff entrances (Toonen et al., 2012). Eventually, the cutoff becomes
232 completely disconnected from the parent channel and forms an oxbow. Based on the presence and

233 position of plug bars in our tidal and fluvial examples, we classified cutoffs into four groups:
234 completely connected, upstream connected, downstream connected, and disconnected (Figure 4).
235 The upstream- and downstream-connected cases can also be merged into a broader category of
236 partially connected cutoffs. Whereas more than 43% of fluvial cutoffs in our dataset are entirely
237 disconnected and only 28% are completely connected (Figure 4a), tidal cutoffs tend to remain
238 connected to their parent channels, with 87% of examples completely connected, 9% partially
239 connected, and only 4% entirely disconnected (Figure 4a).
240 This observed distinction in the connection state of tidal versus fluvial cutoffs appears to be
241 independent of factors such as tidal range, vegetation cover, and geomorphological setting (Figure
242 4). This finding effectively dispels the notion that the absence of plug bars in tidal cutoffs depends
243 on site-specific landscape characteristics (e.g., sediment grain size; Kleinhans et al., 2024).
244 Moreover, similar flow-diversion angles are observed in all our study cases, with median values
245 consistently ranging between 105° and 108° (Figure 4b,c) and further pointing to similar cutoff-
246 triggering mechanisms in fluvial and tidal landscapes. Morphological differences thus can be
247 expected to emerge once cutoffs have formed. The percentage of completely connected fluvial
248 cutoffs decreases as the flow-diversion angle increases, implying that larger Φ_u promote the
249 formation of plug bars and oxbows (Figure 4d). In contrast, tidal cutoffs tend to remain connected
250 to their parent channel irrespective of flow-diversion angles, whether upstream or downstream
251 (Figure 4d and Figure S5 in Supporting Information).
252 Therefore, unlike fluvial analogs, most tidal cutoffs remain hydrodynamically active to some
253 extent: periodic overbank flows in tidal channels result in significant rates of lateral flow injections
254 from the adjoining tidal floodplains during ebb tide, which maintain active flows even in cutoff
255 bends and prevent plug-bar formation by keeping the cutoff entrance flushed. Notably, some tidal
256 cutoffs may also remain connected to other active parts of the network through minor lateral
257 tributaries flowing directly into the cutoff (Figure 1a-i and Figure S6 in Supporting Information).
258 Hence, pronounced hydrological connectivity in tidal wetlands prevents the formation of plug bars
259 and the subsequent evolution of tidal cutoffs into oxbows. Such an evolutionary trajectory clearly
260 differs from fluvial cutoffs, which are typically abandoned and receive water and sediment input
261 almost exclusively during major floods either through minor tie channels carved through the plug
262 bar (Rowland et al., 2009) or as the entire alluvial plain floods (Shen et al., 2021).
263 Among the partially connected cutoffs in our dataset, the fluvial ones are preferentially connected
264 with their parent channels at the upstream end: plug bars tend to form at the cutoff downstream
265 end where flow separations and recirculation create a zone of dead velocity that hinders mixing
266 and promotes sediment deposition (e.g., Turnipseed et al., 2021). In contrast, the few partially
267 connected tidal cutoffs on record, tend to maintain connectivity at the downstream end (Figure 4a),
268 aligned with the direction of typically dominant ebb flows that seemingly keep the cutoff
269 downstream end periodically flushed.

270 *4.3 Meander cutoffs in tidal coastal landscapes: rare or everywhere?*

271 Abundant tidal cutoffs akin to oxbow-rich alluvial floodplains can be found in some tidal settings
272 with possibly lower drainage density and/or sediment supply that limits cutoff infill and vegetation
273 encroachment (Figure 1f-i; Figures S7, S8 in Supporting Information). This further corroborates
274 the observation that tidal and fluvial meandering channels not only evolve through similar
275 morphodynamic processes, but also that tidal meanders are as prone to form cutoffs as their fluvial
276 counterparts given conducive environmental conditions. Given the apparent ubiquity of cutoffs

277 across a variety of tidal environments, why has the notion that sinuous tidal channel bends are
278 inherently unlikely to cut off prevailed for so long (Gabet, 1998; Johnson, 1929)?

279 We suggest that, first, the characteristic width and amplitude of fluvial cutoffs may not vary
280 significantly along a given reach of a meandering river between major tributaries, whereas
281 meander cutoffs within a given tidal wetland can occur across a broad range of meander
282 wavelengths and widths (Finotello, D'Alpaos, et al., 2020). Low-order, narrow tidal creeks are
283 more frequently found than higher-order, wide channels and are thus the most likely to express
284 cutoff development (Figure 1a-i; Figures S7, S8 in Supporting Information). Yet small channels
285 produce small cutoffs, which are especially challenging to observe from a broader spatial vantage,
286 particularly when the vegetation canopy is dense (e.g., in mangrove forests, Figure S9 in
287 Supporting Information).

288 Another consideration is the sustained rate of vertical accretion that characterizes tidal wetlands,
289 coupled with halophytic vegetation that can tolerate significant waterlogging stress. These factors
290 may becloud cutoff traces (Figure 1b,d,f-i and Figure S9 in Supporting Information) through rapid
291 sedimentation in the less hydrodynamically active portions of the cutoff, and the subsequent
292 encroachment of vegetation. This levels out cutoff geomorphic expressions and further hinders
293 their identification from aerial images. Although similar reasoning could apply to fluvial
294 floodplains, reduced overbank sediment supply and slower rates of riparian vegetation growth in
295 permanently waterlogged areas may prolong the timescale required to fill oxbows, making large
296 river-cutoff scars identifiable from aerial photos for much longer periods (Kleinhans et al., 2024)
297 (Figure 1j,k).

298 The apparent absence of tidal cutoffs is thus more an artifact of observations than a consequence
299 of physical mechanisms. High drainage densities in tidal wetlands surely constrain the freely
300 meandering of tidal channels (Figure S10 in Supporting Information). Yet the relatively small size
301 of most tidal channels, along with the distinctive hydrological characteristics of tidal wetlands,
302 contribute to the transient nature of tidal cutoffs and make them challenging to record. That is,
303 unlike other features of meandering channels that might jump out at the observer, to find tidal
304 cutoffs one has to go carefully looking for them.

305 The implied morphodynamic similarity between tidal and fluvial meanders is by no means
306 diminished by the absence of prominent scroll bars in tidal wetlands, standing in stark contrast to
307 river floodplains that often – but not always (Candel et al., 2020, 2021) – showcase intricate
308 arrangements of sub-parallel scrolls indicative of previous channel locations (Figure 1k) (Strick et
309 al., 2018). While there is no consensus on what drives the formation of scroll bars (van de Lageweg
310 et al., 2014), we offer two possible, not mutually exclusive explanations for the absence of scroll
311 bars in tidal meanders. One possibility is that tidal meanders undergo small and yet continuous
312 incremental migrations, unlike fluvial meanders which tend to migrate more episodically during
313 major flood events (Mason & Mohrig, 2019; Wu et al., 2016). Another hypothesis is that sustained
314 rates of vertical aggradation relative to lateral channel migration in tidal wetlands prevent scroll
315 bars by systematically overshadowing any topographic irregularities (Brivio et al., 2016; Cosma
316 et al., 2019). This explanation aligns with the lack of scroll bars in meandering streamflows
317 evolving through curvature-driven fluvial-like mechanisms in aggradational settings such as
318 coastal backwater areas (Swartz et al., 2020), peatlands (Candel et al., 2017), and submarine
319 turbidity-current channels (Jobe et al., 2016; Morris et al., 2024).

320 **5 Implications and Conclusions**

321 Our findings demonstrate that meandering channels in tidal wetlands possess the same capacity

322 to form meander cutoffs as their fluvial counterparts. The morphometric evidence we have
323 gathered suggests that the morphodynamic processes driving the development of both tidal and
324 fluvial cutoffs are fundamentally similar. However, substantial differences arise after cutoffs have
325 formed. Unlike fluvial cutoffs, which tend to form oxbows, tidal cutoffs remain preferentially
326 connected to their parent channel. This distinction is attributed to the pronounced hydrological
327 connectivity characteristic of tidal wetlands. As a result, tidal meander cutoffs continue to actively
328 participate in the draining and flooding of the surrounding wetlands, and maintain their status as
329 integral components of the overall system.

330 Considered alongside previous studies, our results indicate a complete morphodynamic analogy
331 between tidal and fluvial meandering channels from meander inception to cutoff (Finotello et al.,
332 2018, 2022; Gao, Finotello, & Wang, 2022; Leuven et al., 2018). The unification of tidal and
333 fluvial meander morphodynamics allows for extending classical techniques for modeling
334 meandering rivers (Bogoni et al., 2017; Howard & Knutson, 1984; Parker et al., 2011; Seminara
335 et al., 2001) to tidal wetland contexts, where meandering is ubiquitous and yet routinely omitted.
336 Such an advance in numerical modeling would open new opportunities for how researchers model
337 tidal wetland ecomorphodynamics, with important implications for the effective conservation and
338 restoration of these critical ecosystems.

339 **Acknowledgments**

340 We are grateful for constructive reviews from M. Kleinhans and one anonymous reviewer, as well
341 as for recommendations from the Editorial Office, which improved this manuscript.

342 This study is funded by the European Union – NextGenerationEU and by the University of Padua
343 under the 2021 STARS Grants@Unipd programme "TiDyLLy- Tidal networks dynamics as
344 drivers for ecomorphodynamics of low-lying coastal area" (to AF), as well as by a China
345 Scholarship Council (CSC) scholarships (202106190084, to CG). AI is supported by a Discovery
346 Grant from the Natural Sciences and Engineering Research Council of Canada. AF, MG, and ADA
347 also acknowledge support by the Italian Ministry of University and Research (MUR) through the
348 project titled 'The Geosciences for Sustainable Development' (Budget MUR - Dipartimenti di
349 Eccellenza 2023-2027; Project ID C93C23002690001)

350 **Conflict of Interest Statement**

351 The authors declare no conflict of interest.

352 **Open Research**

353 All the data presented and analyzed in this paper are freely available from a public Zenodo folder
354 (Gao & Finotello, 2023)

355 **References**

- 356 Bogoni, M., Putti, M., & Lanzoni, S. (2017). Modeling meander morphodynamics over self-
357 formed heterogeneous floodplains. *Water Resources Research*, 53(6), 5137–5157.
358 <https://doi.org/10.1002/2017WR020726>
- 359 Brivio, L., Ghinassi, M., D'Alpaos, A., Finotello, A., Fontana, A., Roner, M., & Howes, N. (2016).
360 Aggradation and lateral migration shaping geometry of a tidal point bar: An example from
361 salt marshes of the Northern Venice Lagoon (Italy). *Sedimentary Geology*, 343, 141–155.
362 <https://doi.org/10.1016/j.sedgeo.2016.08.005>
- 363 Camporeale, C., Perona, P., Porporato, A., & Ridolfi, L. (2005). On the long-term behavior of
364 meandering rivers. *Water Resources Research*, 41(12), 1–13.

365 <https://doi.org/10.1029/2005WR004109>
366 Candel, J. H. J., Makaske, B., Storms, J. E. A., & Wallinga, J. (2017). Oblique aggradation: a novel
367 explanation for sinuosity of low-energy streams in peat-filled valley systems. *Earth Surface*
368 *Processes and Landforms*, 42(15), 2679–2696. <https://doi.org/10.1002/esp.4100>
369 Candel, J. H. J., Makaske, B., Kijm, N., Kleinhans, M. G., Storms, J. E. A., & Wallinga, J. (2020).
370 Self-constraining of low-energy rivers explains low channel mobility and tortuous planforms.
371 *Depositional Record*, 6(3), 648–669. <https://doi.org/10.1002/dep2.112>
372 Candel, J. H. J., Kleinhans, M. G., Makaske, B., & Wallinga, J. (2021). Predicting river channel
373 pattern based on stream power, bed material and bank strength. *Progress in Physical*
374 *Geography*, 45(2), 253–278. <https://doi.org/10.1177/0309133320948831>
375 Constantine, J. A., & Dunne, T. (2008). Meander cutoff and the controls on the production of
376 oxbow lakes. *Geology*, 36(1), 23–26. <https://doi.org/10.1130/G24130A.1>
377 Cosma, M., Ghinassi, M., D’Alpaos, A., Roner, M., Finotello, A., Tommasini, L., & Gatto, R.
378 (2019). Point-bar brink and channel thalweg trajectories depicting interaction between
379 vertical and lateral shifts of microtidal channels in the Venice Lagoon (Italy).
380 *Geomorphology*, 342, 37–50. <https://doi.org/10.1016/j.geomorph.2019.06.009>
381 Cosma, M., Finotello, A., Ielpi, A., Ventra, D., Oms, O., D’Alpaos, A., & Ghinassi, M. (2020).
382 Piracy-controlled geometry of tide-dominated point bars: Combined evidence from ancient
383 sedimentary successions and modern channel networks. *Geomorphology*, 370, 107402.
384 <https://doi.org/10.1016/j.geomorph.2020.107402>
385 Dieras, P. L. (2013). The Persistence of Oxbow Lakes as Aquatic Habitats : an Assessment of
386 Rates of Change and Patterns of Alluviation Doctorate of Philosophy, 177. Retrieved from
387 <http://orca.cf.ac.uk/49392/>
388 Dunne, T., & Aalto, R. E. (2013). Large River Floodplains. In J. E. Schroder & E. Wohl (Eds.),
389 *Treatise on Geomorphology* (Vol. 9, pp. 645–678). Elsevier. [https://doi.org/10.1016/B978-0-](https://doi.org/10.1016/B978-0-12-374739-6.00258-X)
390 [12-374739-6.00258-X](https://doi.org/10.1016/B978-0-12-374739-6.00258-X)
391 Fagherazzi, S., Gabet, E. J., & Furbish, D. J. (2004). The effect of bidirectional flow on tidal
392 channel planforms. *Earth Surface Processes and Landforms*, 29(3), 295–309.
393 <https://doi.org/10.1002/esp.1016>
394 Finotello, A., Lanzoni, S., Ghinassi, M., Marani, M., Rinaldo, A., & D’Alpaos, A. (2018). Field
395 migration rates of tidal meanders recapitulate fluvial morphodynamics. *Proceedings of the*
396 *National Academy of Sciences*, 115(7), 1463–1468. <https://doi.org/10.1073/pnas.1711330115>
397 Finotello, A., D’Alpaos, A., Bogoni, M., Ghinassi, M., & Lanzoni, S. (2020). Remotely-sensed
398 planform morphologies reveal fluvial and tidal nature of meandering channels. *Scientific*
399 *Reports*, 10(1), 1–13. <https://doi.org/10.1038/s41598-019-56992-w>
400 Finotello, A., Ghinassi, M., Carniello, L., Belluco, E., Pivato, M., Tommasini, L., & D’Alpaos, A.
401 (2020). Three-Dimensional Flow Structures and Morphodynamic Evolution of Microtidal
402 Meandering Channels. *Water Resources Research*, 56(7), e2020WR027822.
403 <https://doi.org/10.1029/2020WR027822>
404 Finotello, A., Capperucci, R. M., Bartholomä, A., D’Alpaos, A., & Ghinassi, M. (2022). Morpho-
405 sedimentary evolution of a microtidal meandering channel driven by 130 years of natural and
406 anthropogenic modifications of the Venice Lagoon (Italy). *Earth Surface Processes and*
407 *Landforms*, 47(10), 2580–2596. <https://doi.org/10.1002/esp.5396>
408 Frascati, A., & Lanzoni, S. (2009). Morphodynamic regime and long-term evolution of
409 meandering rivers. *Journal of Geophysical Research: Earth Surface*, 114(2), 1–12.
410 <https://doi.org/10.1029/2008JF001101>

411 Gabet, E. J. (1998). Lateral Migration and Bank Erosion in a Saltmarsh Tidal Channel in San
412 Francisco Bay, California. *Estuaries*, 21(4), 745. <https://doi.org/10.2307/1353278>

413 Gao, C., & Finotello, A. (2023). Morphometry of widespread tidal meander cutoffs discloses
414 similarity to fluvial morphodynamics. [Dataset]. <https://doi.org/10.5281/zenodo.8229300>

415 Gao, C., Finotello, A., D'Alpaos, A., Ghinassi, M., Carniello, L., Pan, Y., et al. (2022).
416 Hydrodynamics of Meander Bends in Intertidal Mudflats: A Field Study From the Macrotidal
417 Yangkou Coast, China. *Water Resources Research*, 58(12), 1–28.
418 <https://doi.org/10.1029/2022WR033234>

419 Gao, C., Finotello, A., & Wang, Y. P. (2022). Predominant landward skewing of tidal meanders.
420 *Earth Surface Processes and Landforms*, (July), 1–17. <https://doi.org/10.1002/esp.5452>

421 Gasparotto, A., Darby, S. E., Leyland, J., & Carling, P. A. (2022). Water level fluctuations drive
422 bank instability in a hypertidal estuary. *Earth Surface Dynamics*, 2080(September), 1–28.

423 Hayden, A. T., Lamb, M. P., & Carney, A. J. (2021). Similar curvature-to-width ratios for channels
424 and channel belts: Implications for paleo-hydraulics of fluvial ridges on Mars. *Geology*,
425 49(7), 837–841. <https://doi.org/10.1130/G48370.1>

426 Hooke, J. M. (2013). River Meandering. In E. Wohl & Schroder (Eds.), *Treatise on*
427 *Geomorphology* (Vol. 9, pp. 260–288). Washington: Elsevier. <https://doi.org/10.1016/B978-0-12-374739-6.00241-4>

429 Howard, A. D., & Hemberger, A. T. (1991). Multivariate characterization of meandering.
430 *Geomorphology*, 4(3–4), 161–186. [https://doi.org/10.1016/0169-555X\(91\)90002-R](https://doi.org/10.1016/0169-555X(91)90002-R)

431 Howard, A. D., & Knutson, T. R. (1984). Sufficient conditions for river meandering: A simulation
432 approach. *Water Resources Research*, 20(11), 1659–1667.
433 <https://doi.org/10.1029/WR020i011p01659>

434 Hughes, Z. J. (2012). Tidal channels on tidal flats and marshes. In R. A. Davis & R. W. Dalrymple
435 (Eds.), *Principles of Tidal Sedimentology* (Springer, pp. 269–300). Dordrecht: Springer.
436 https://doi.org/10.1007/978-94-007-0123-6_11

437 Jobe, Z. R., Howes, N. C., & Auchter, N. C. (2016). Comparing submarine and fluvial channel
438 kinematics: Implications for stratigraphic architecture. *Geology*, 44(11), 931–934.
439 <https://doi.org/10.1130/G38158.1>

440 Johnson, D. (1929). Meanders in Tidal Streams: A Review and Discussion. *Geographical Review*,
441 19(1), 135. <https://doi.org/10.2307/208081>

442 Kearney, W. S., & Fagherazzi, S. (2016). Salt marsh vegetation promotes efficient tidal channel
443 networks. *Nature Communications*, 7, 1–7. <https://doi.org/10.1038/ncomms12287>

444 Kleinhans, M. G., Schuurman, F., Bakx, W., & Markies, H. (2009). Meandering channel dynamics
445 in highly cohesive sediment on an intertidal mud flat in the Westerschelde estuary, the
446 Netherlands. *Geomorphology*, 105(3–4), 261–276.
447 <https://doi.org/10.1016/j.geomorph.2008.10.005>

448 Kleinhans, M. G., McMahon, W. J., & Davies, N. S. (2024). What even is a meandering river? A
449 philosophy-enhanced synthesis of multilevel causes and systemic interactions contributing to
450 river meandering. *Geological Society, London, Special Publications*, 540(1).
451 <https://doi.org/10.1144/sp540-2022-138>

452 van de Lageweg, W. I., van Dijk, W. M., Baar, A. W., Rutten, J., & Kleinhans, M. G. (2014). Bank
453 pull or bar push: What drives scroll-bar formation in meandering rivers? *Geology*, 42(4), 319–
454 322. <https://doi.org/10.1130/G35192.1>

455 Leopold, L. B., Wolman, M. G., & Miller, J. P. (1964). *Fluvial processes in geomorphology*
456 (Freeman). San Francisco. Retrieved from <http://catalogue.nla.gov.au/Record/2338901>

- 457 Letzsch, W. S., & Frey, R. W. (1980). Deposition and erosion in a Holocene salt marsh, Sapelo
458 Island, Georgia. *Journal of Sedimentary Petrology*, 50(2), 529–542.
459 <https://doi.org/10.1306/212F7A45-2B24-11D7-8648000102C1865D>
- 460 Leuven, J. R. F. W., Kleinhans, M. G., Weisscher, S. A. H., & van der Vegt, M. (2016). Tidal sand
461 bar dimensions and shapes in estuaries. *Earth-Science Reviews*, 161, 204–223.
462 <https://doi.org/10.1016/j.earscirev.2016.08.004>
- 463 Leuven, J. R. F. W., van Maanen, B., Lexmond, B. R., van der Hoek, B. V., Spruijt, M. J., &
464 Kleinhans, M. G. (2018). Dimensions of fluvial-tidal meanders: Are they disproportionately
465 large? *Geology*, 46(10), 923–926. <https://doi.org/10.1130/G45144.1>
- 466 Li, Z., Gao, P., You, Y., Finotello, A., & Ielpi, A. (2022). Delayed neck cutoff in the meandering
467 Black River of the Qinghai–Tibet plateau. *Earth Surface Processes and Landforms*,
468 (September 2022), 1–12. <https://doi.org/10.1002/esp.5534>
- 469 Marani, M., Belluco, E., D’Alpaos, A., Defina, A., Lanzoni, S., & Rinaldo, A. (2003). On the
470 drainage density of tidal networks. *Water Resources Research*, 39(2), 1–11.
471 <https://doi.org/10.1029/2001WR001051>
- 472 Mason, J., & Mohrig, D. (2019). Scroll bars are inner bank levees along meandering river bends.
473 *Earth Surface Processes and Landforms*, 44(13), 2649–2659.
474 <https://doi.org/10.1002/esp.4690>
- 475 Morris, P. D., Sylvester, Z., Covault, J. A., Mohrig, D., & Dunlap, D. (2024). Fluvial-style
476 migration controls autogenic aggradation in submarine channels: Joshua Channel, eastern
477 Gulf of Mexico. In A. Finotello, Z. Sylvester, & P. R. Durkin (Eds.), *Meandering*
478 *Streamflows: Patterns and Processes across Landscapes and Scales* (Vol. 540). Geological
479 Society, London, Special Publications. <https://doi.org/10.1144/SP540-2022-123>
- 480 Parker, G., Shimizu, Y., Wilkerson, G. V., Eke, E. C., Abad, J. D., Lauer, J. W., et al. (2011). A
481 new framework for modeling the migration of meandering rivers. *Earth Surface Processes*
482 *and Landforms*, 36(1), 70–86. <https://doi.org/10.1002/esp.2113>
- 483 Rowland, J. C., Dietrich, W. E., Day, G., & Parker, G. (2009). Formation and maintenance of
484 single-thread tie channels entering floodplain lakes: Observations from three diverse river
485 systems. *Journal of Geophysical Research: Earth Surface*, 114(2), 1–19.
486 <https://doi.org/10.1029/2008JF001073>
- 487 Schumm, S. A., Erskine, W. D., & Tilleard, J. W. (1996). Morphology, hydrology, and evolution
488 of the anastomosing Ovens and King Rivers, Victoria, Australia. *Bulletin of the Geological*
489 *Society of America*, 108(10), 1212–1224. [https://doi.org/10.1130/0016-7606\(1996\)108<1212:MHAEOT>2.3.CO;2](https://doi.org/10.1130/0016-7606(1996)108<1212:MHAEOT>2.3.CO;2)
- 491 Schwarz, C., van Rees, F., Xie, D., Kleinhans, M. G., & van Maanen, B. (2022). Salt marshes
492 create more extensive channel networks than mangroves. *Nature Communications*, 13(1),
493 2017. <https://doi.org/10.1038/s41467-022-29654-1>
- 494 Schwenk, J., Lanzoni, S., & Fofoula-Georgiou, E. (2015). The life of a meander bend: Connecting
495 shape and dynamics via analysis of a numerical model. *Journal of Geophysical Research:*
496 *Earth Surface*, 120(4), 690–710. <https://doi.org/10.1002/2014JF003252>
- 497 Seminara, G., Zolezzi, G., Tubino, M., & Zardi, D. (2001). Downstream and upstream influence
498 in river meandering. Part 2. Planimetric development. *Journal of Fluid Mechanics*, 438, 213–
499 230. <https://doi.org/10.1017/S0022112001004281>
- 500 Shen, Z., Aeschliman, M., & Conway, N. (2021). Paleodischarge reconstruction using oxbow lake
501 sediments complicated by shifting hydrological connectivity. *Quaternary International*,
502 604(July), 75–81. <https://doi.org/10.1016/j.quaint.2021.07.004>

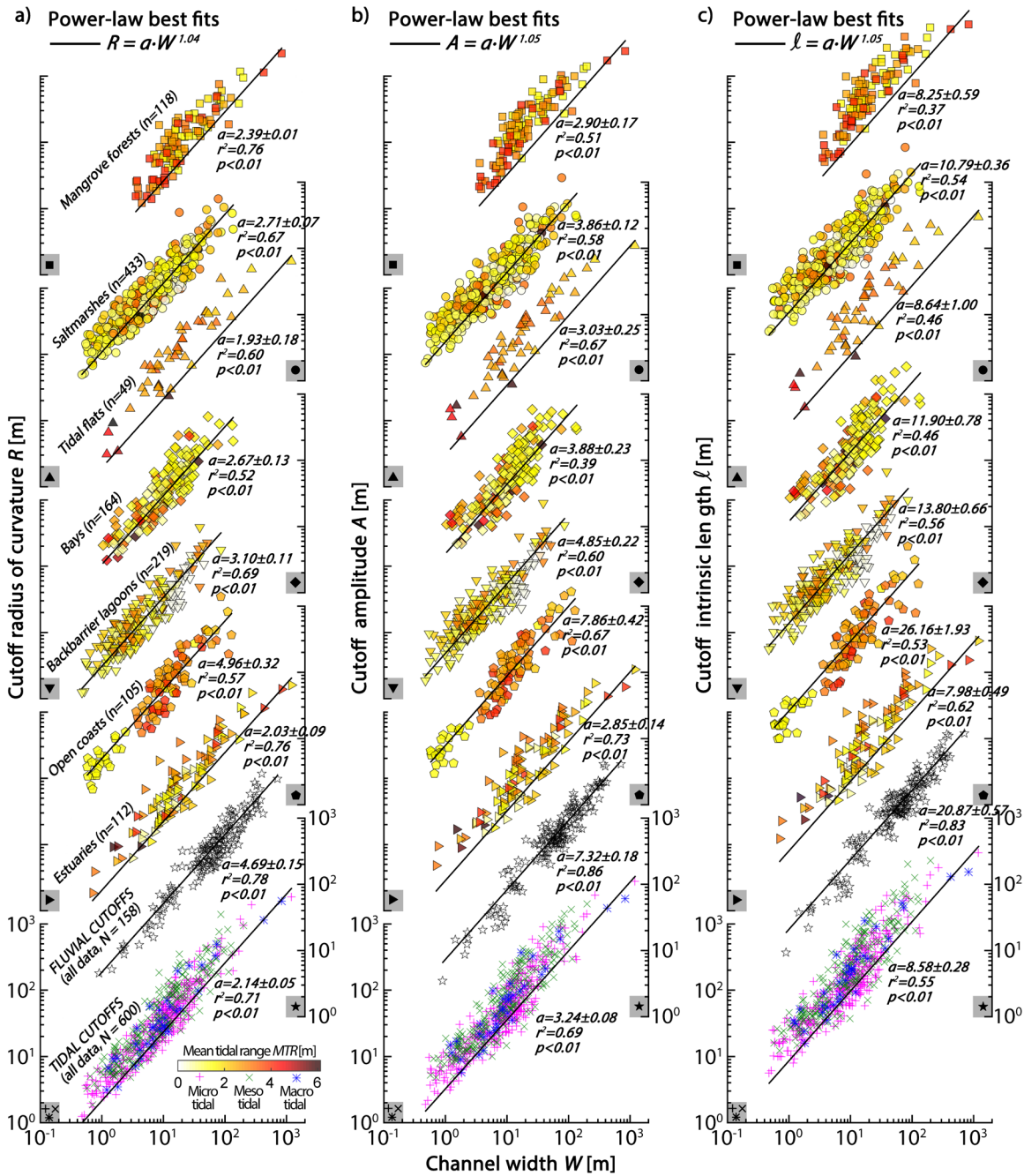
- 503 Solari, L., Seminara, G., Lanzoni, S., Marani, M., & Rinaldo, A. (2002). Sand bars in tidal channels
504 part 2. Tidal meanders. *Journal of Fluid Mechanics*, 451(January), 203–238.
505 <https://doi.org/10.1017/s0022112001006565>
- 506 Stølum, H. H. (1996). River meandering as a self-organization process. *Science*, 271(5256), 1710–
507 1713. <https://doi.org/10.1126/science.271.5256.1710>
- 508 Strick, R. J. P., Ashworth, P. J., Awcock, G., & Lewin, J. (2018). Morphology and spacing of river
509 meander scrolls. *Geomorphology*, 310, 57–68.
510 <https://doi.org/10.1016/j.geomorph.2018.03.005>
- 511 Swartz, J. M., Goudge, T. A., & Mohrig, D. C. (2020). Quantifying Coastal Fluvial
512 Morphodynamics Over the Last 100 Years on the Lower Rio Grande, USA and Mexico.
513 *Journal of Geophysical Research: Earth Surface*, 125(6), 1–16.
514 <https://doi.org/10.1029/2019JF005443>
- 515 Thomas, S. S., Constantine, J. A., Dethier, D., Thoman, J. W., Racela, J., Blau, E., & Landis, J. D.
516 (2022). The importance of oxbow lakes in the floodplain storage of pollutants. *Geology*,
517 50(4), 392–396. <https://doi.org/10.1130/G49427.1>
- 518 Toonen, W. H. J., Kleinhans, M. G., & Cohen, K. M. (2012). Sedimentary architecture of
519 abandoned channel fills. *Earth Surface Processes and Landforms*, 37(4), 459–472.
520 <https://doi.org/10.1002/esp.3189>
- 521 Torres, M. A., Limaye, A. B., Ganti, V., Lamb, M. P., Joshua West, A., & Fischer, W. W. (2017).
522 Model predictions of long-lived storage of organic carbon in river deposits. *Earth Surface*
523 *Dynamics*, 5(4), 711–730. <https://doi.org/10.5194/esurf-5-711-2017>
- 524 Turnipseed, C., Konsoer, K., Richards, D., & Willson, C. (2021). Numerical Modeling of Two-
525 Dimensional Hydrodynamics in a Highly Curving and Actively Evolving Neck Cutoff Under
526 Different Hydrologic Conditions. *Water Resources Research*, 57(2), 1–14.
527 <https://doi.org/10.1029/2020WR027329>
- 528 Vermeulen, B., Hoitink, A. J. F., Zolezzi, G., Abad, J. D., & Aalto, R. (2016). Multiscale structure
529 of meanders. *Geophysical Research Letters*, 43(7), 3288–3297.
530 <https://doi.org/10.1002/2016GL068238>
- 531 Vilas, F., Arche, A., Ferrero, M., & Isla, F. (1999). Subantarctic macrotidal flats, cheniers and
532 beaches in San Sebastian Bay, Tierra Del Fuego, Argentina. *Marine Geology*, 160(3–4), 301–
533 326. [https://doi.org/10.1016/S0025-3227\(99\)00021-3](https://doi.org/10.1016/S0025-3227(99)00021-3)
- 534 Wu, C., Ullah, M. S., Lu, J., & Bhattacharya, J. P. (2016). Formation of point bars through rising
535 and falling flood stages: Evidence from bar morphology, sediment transport and bed shear
536 stress. *Sedimentology*, 63(6), 1458–1473. <https://doi.org/10.1111/sed.12269>
- 537 Zhao, K., Coco, G., Gong, Z., Darby, S. E., Lanzoni, S., Xu, F., et al. (2022). A Review on Bank
538 Retreat: Mechanisms, Observations, and Modeling. *Reviews of Geophysics*, 60(2), 1–51.
539 <https://doi.org/10.1029/2021rg000761>
- 540 Zinger, J. A., Rhoads, B. L., & Best, J. L. (2011). Extreme sediment pulses generated by bend
541 cutoffs along a large meandering river. *Nature Geoscience*, 4(10), 675–678.
542 <https://doi.org/10.1038/ngeo1260>
- 543
- 544



546
 547 **Figure 1. Meander cutoffs in tidal and fluvial landscapes.** (a,b,c,d) Examples of individual tidal meander
 548 cutoffs from distinct coastal settings worldwide (image© Google, Maxar). (f,g,h,i) Examples of tidal
 549 environments characterized by widespread meander cutoffs (image©Google: TerraMetrics, CNES/Airbus,

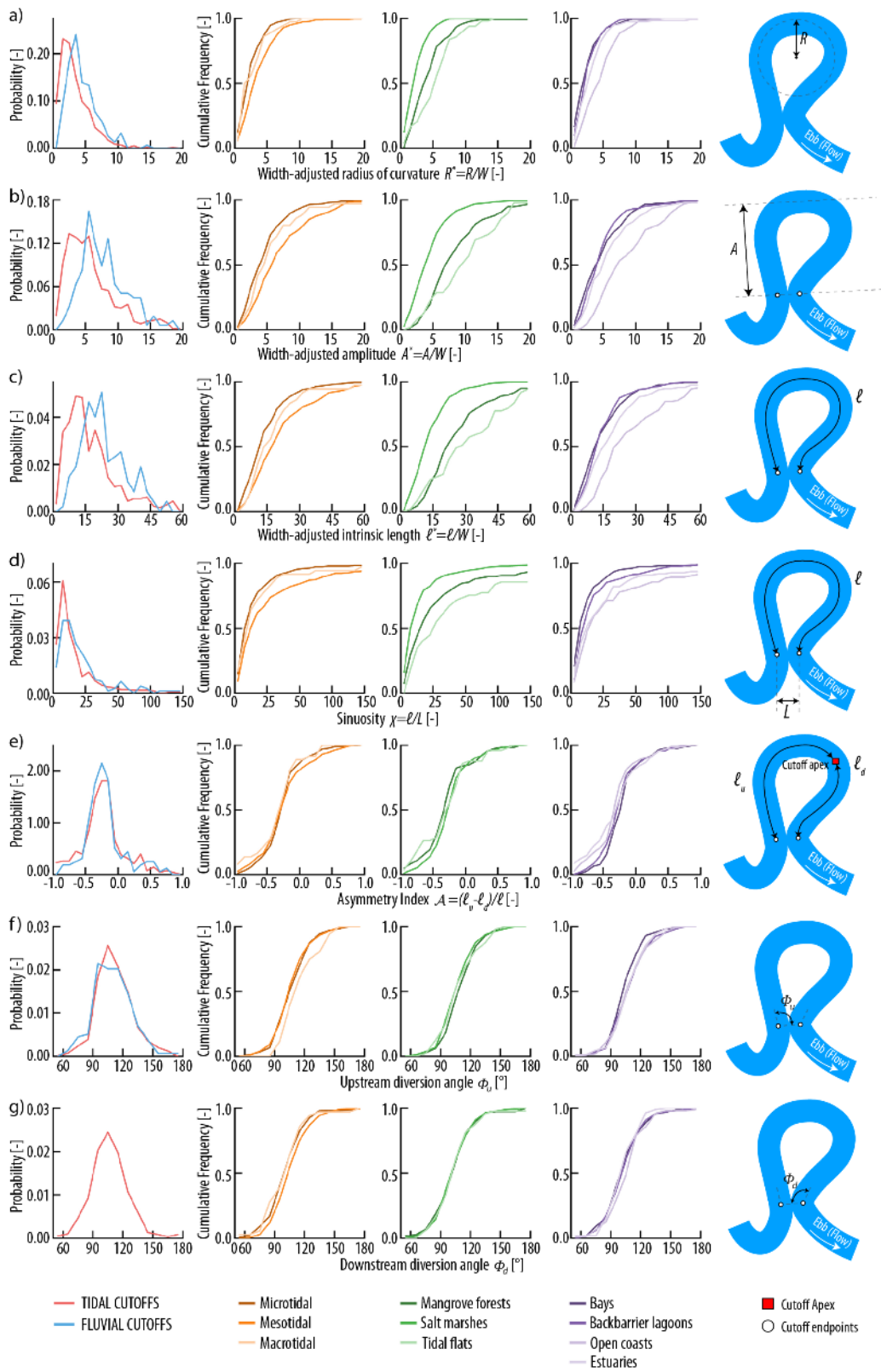
550 Maxar, Landsat/Copernicus). (j,k) Examples of river floodplains littered by oxbow lakes and cutoff traces
551 (image©Google: Maxar). Geographic coordinates are reported in each panel. Dotted red and blue lines
552 highlight discernable traces of meander cutoffs in tidal and fluvial landscapes, respectively. l) Sketch
553 illustrating the main morphometric features of meander cutoffs analyzed in this study.

554



556
 557
 558
 559
 560
 561
 562
 563
 564

Figure 2. Cutoff morphometrics. Cutoff radius of curvature (R), Amplitude (A), and intrinsic length (l) are plotted against channel width (W) both separately for all tidal and fluvial cutoffs on record and for different tidal-cutoff ensembles based on geomorphological settings and vegetation cover color-coded based on tidal ranges. Continuous black lines represent best-fit power law regressions obtained for different data ensembles, using a common exponent derived from all data and applied to calculate scaling coefficients for each ensemble. Note that the vertical offset among individual data plots is arbitrary: each vertical y-axis ranges from 10^0 to 10^3 , and symbols are positioned at the bottom of the axis to aid in identifying the corresponding data plot.

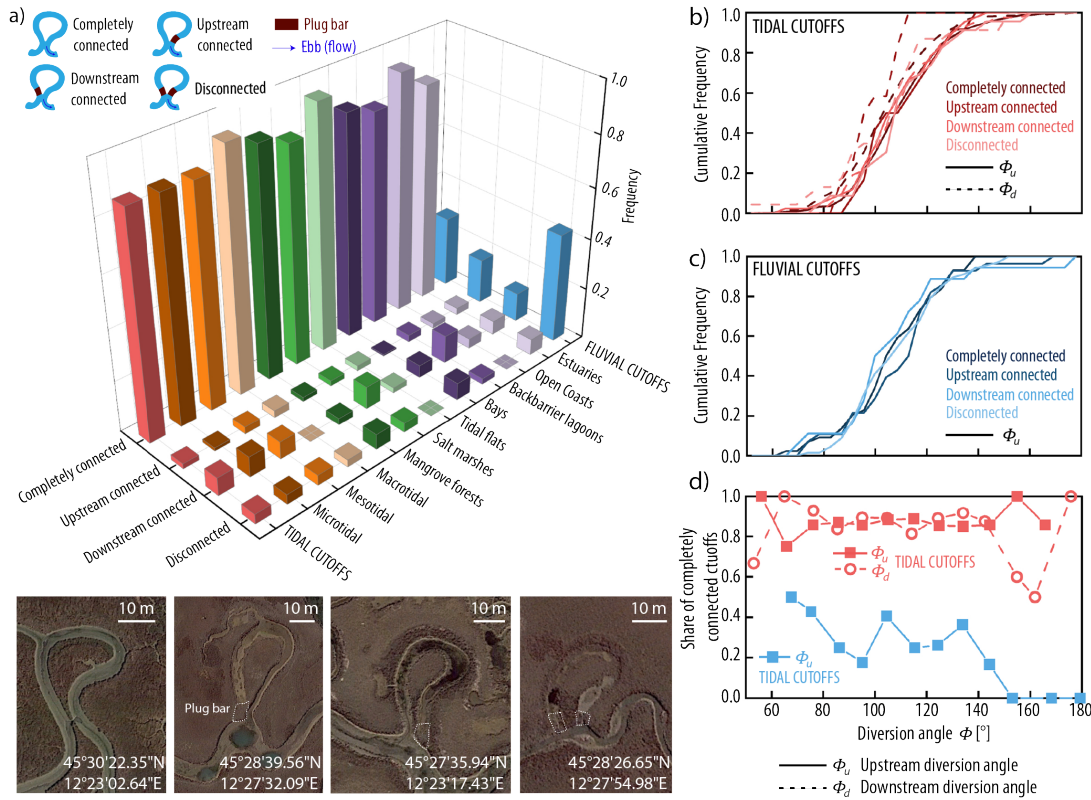


565
566
567

Figure 3. Dimensionless cutoff morphometrics. (a) Width-adjusted radius of curvature; (b) width-adjusted amplitude (c) width-adjusted intrinsic length; (d) sinuosity (χ); (e) asymmetry index (\mathcal{A}); (f,g)

568 upstream and downstream flow-diversion angles (Φ_u and Φ_d). Panels in the first column show empirical
569 probability distributions for tidal (red) and fluvial (blue) cutoffs. Panels in the other columns report
570 empirical cumulative frequency distributions for tidal cutoffs subdivided based on tidal range, vegetation
571 cover, and geomorphological setting. The fifth column contains sketch-up views for each investigated
572 morphometric.

573



575
576
577
578
579
580
581
582
583
584

Figure 4. Cutoff connectivity. (a) Barplot showing the relative frequency of different connection types between cutoffs and parent channels, differentiating tidal (red) and fluvial (blue) cutoffs, and further segmenting tidal cutoff ensembles based on tidal range (orange), vegetation cover (green), and geomorphological settings (purple). (b,c) Frequency distributions of flow-diversion angles (Φ) for tidal and fluvial cutoffs. Different colors denote different connectivity with the parent channel. Solid and dashed lines denote upstream and downstream diversion angles, respectively. (d) Share of completely connected tidal (red) and fluvial (blue) cutoffs across uniform 10° diversion-angle intervals. Solid squares and empty dots denote upstream and downstream diversion angles, respectively. (e) Tidal cutoffs found in the microtidal lagoon of Venice (Italy) characterized by different connectivity.

Supporting Information for

Morphometry of tidal meander cutoffs indicates similarity to fluvial morphodynamics

*C. Gao^{1,2}, E. D. Lazarus³, A. D'Alpaos², M. Ghinassi², A. Ielpi⁴, G. Parker^{5,6}, A. Rinaldo^{7,8}, P. Gao⁹,
Y. P. Wang^{1,10}, D. Tognin⁷, and A. Finotello^{2*}*

1) Ministry of Education Key Laboratory for Coast and Island Development, School of Geographic and Oceanographic Sciences, Nanjing University, Nanjing, China.

2) Department of Geosciences, University of Padova, Padova, Italy.

3) School of Geography & Environmental Science, University of Southampton, Southampton, UK.

4) Department of Earth, Environmental and Geographic Sciences, University of British Columbia-Okanagan, Kelowna, BC, Canada

5) Department of Civil & Environmental Engineering, University of Illinois, Urbana-Champaign, IL, USA

6) Department of Geology, University of Illinois, Urbana-Champaign, IL, USA

7) Department of Civil, Architectural and Environmental Engineering, University of Padova, Padova, Italy

8) Laboratory of Ecohydrology, École Polytechnique Fédérale de Lausanne, Lausanne, Switzerland

9) Department of Geography and the Environment, Syracuse University, Syracuse, NY, USA

10) State Key Laboratory of Estuarine and Coastal Research, School of Marine Sciences, East China Normal University, Shanghai, China

**Corresponding author: Alvise Finotello (alvise.finotello@unipd.it)*

Contents of this file

Figures S1 to S10

Tables S1 to S13



Figure S1. Examples of tidal cutoffs found in tidal environments characterized by different tidal regimes, vegetation coverages, and geomorphological settings.

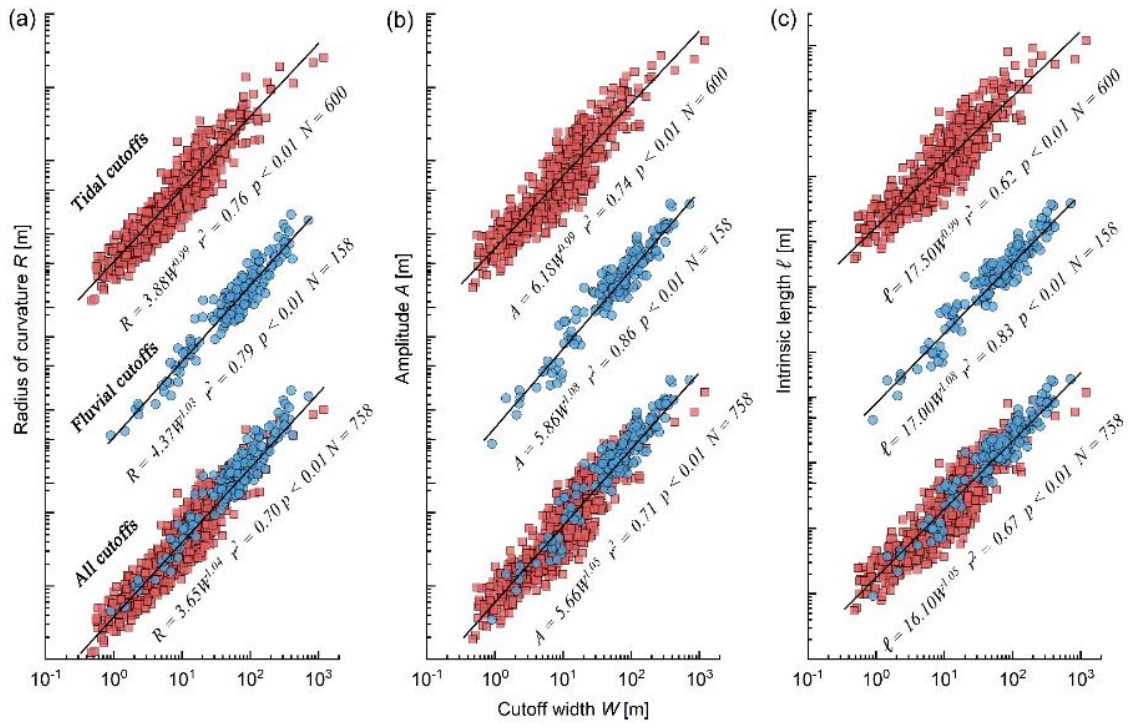


Figure S2. Planform morphometrics of tidal and fluvial meander cutoffs. The cutoff radius of curvature (R), Amplitude (A), and intrinsic length (ℓ) are plotted against channel width (W). Data are plotted both separately and altogether for tidal (red) and fluvial cutoffs (blue). Note that the vertical offset is arbitrary. Continuous black lines represent best-fit power law regressions for each set of data points.

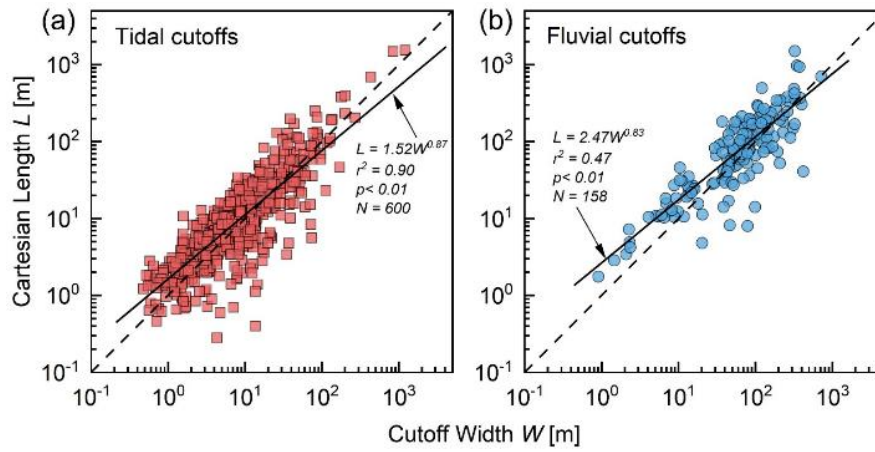


Figure S3. Relationship between cutoff Cartesian length (L) and channel width (W) for (a) tidal and (b) fluvial cutoffs, respectively. The solid lines represent the power-law best fits for all data, whereas dashed lines denote $L = W$.



Figure S4. Examples of tidal channel piracies (i.e., captures) from different tidal environments worldwide. a,b,c,) Pagliaga salt marsh, Venice Lagoon, Italy (image ©Google, unknown). d) Ile aux Oiseaux, Aranchon Bay, France (image ©Google, unknown). e) Willapa River, Washington, USA (image ©Google, unknown). f) Hampton, New Hampshire, USA (image ©Google, unknown). g) Pyin Ah Lan/Poe Laung, Myanmar (image ©Google, Maxar technologies). h) Irawaddy River Delta, Myanmar (image ©Google, Maxar technologies). i) Rope River Estuary, Northern Territory, Australia (image ©Google, Maxar technologies). j) Cape Romain National Wildlife Refuge, South Carolina, USA (image ©Google, unknown).

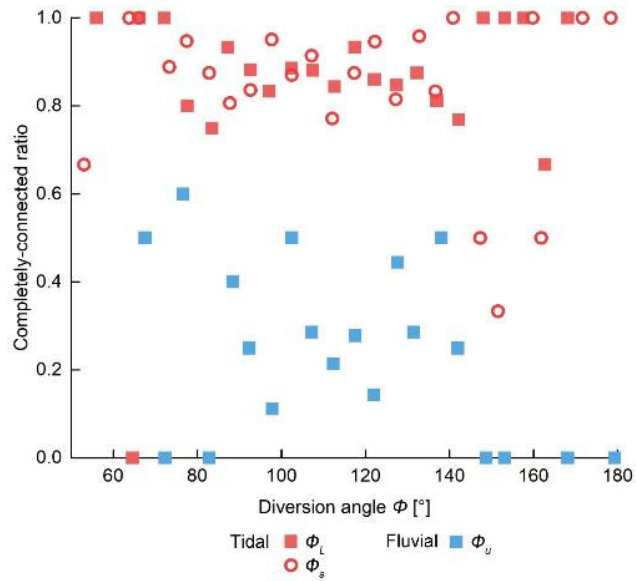


Figure S5. Shares of completely connected cutoffs as a function of diversion angle, computed by binning data based on equally spaced Φ interval (bin size = 5°) and then dividing the number of completely connected cutoffs by the total number of cutoffs in each interval. Tidal and fluvial cutoff data are plotted in red and blue colors, with solid squares and empty dots denoting upstream and downstream diversion angles, respectively.

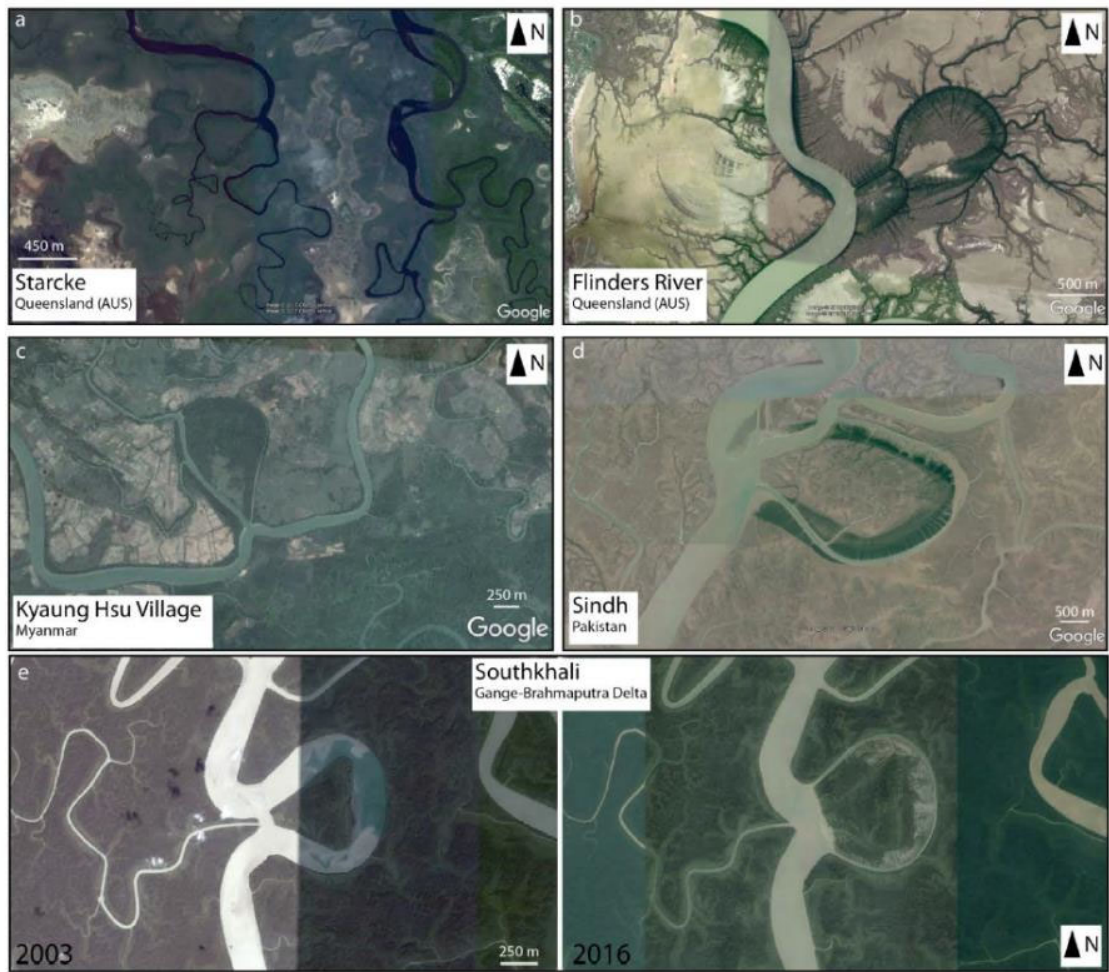


Figure S6. Examples of tidal cutoff remaining either partially or completely connected to their parent channels while keep draining water from the surrounding intertidal areas.

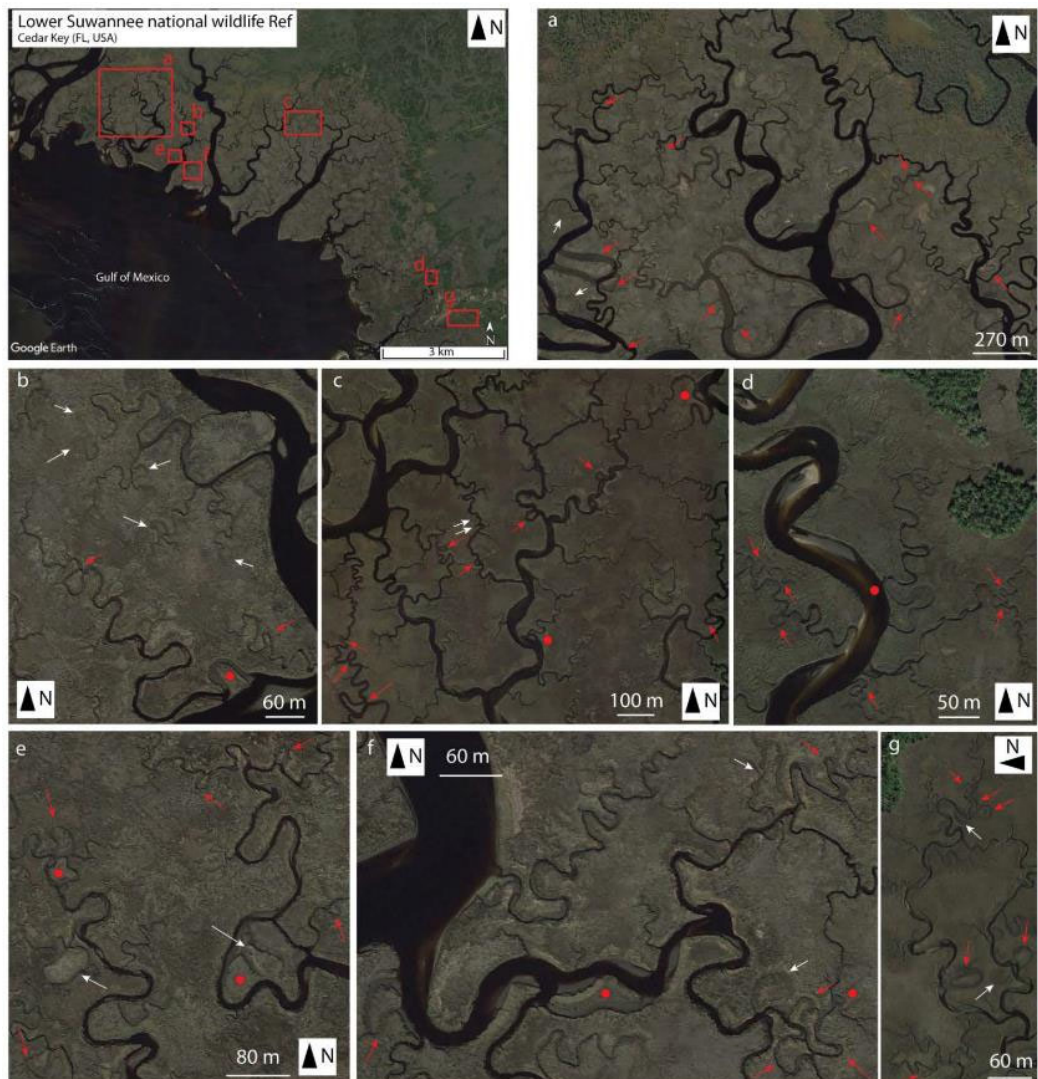


Figure S7. Identification of tidal meander cutoffs within the lower Suwannee National wildlife Ref (FL, USA). Red and white arrows indicate active and relic (i.e., unanalyzed) cutoffs, respectively, whereas red dots identify abandoned channels produced by piracies (i.e., captures) of two adjoining channels.

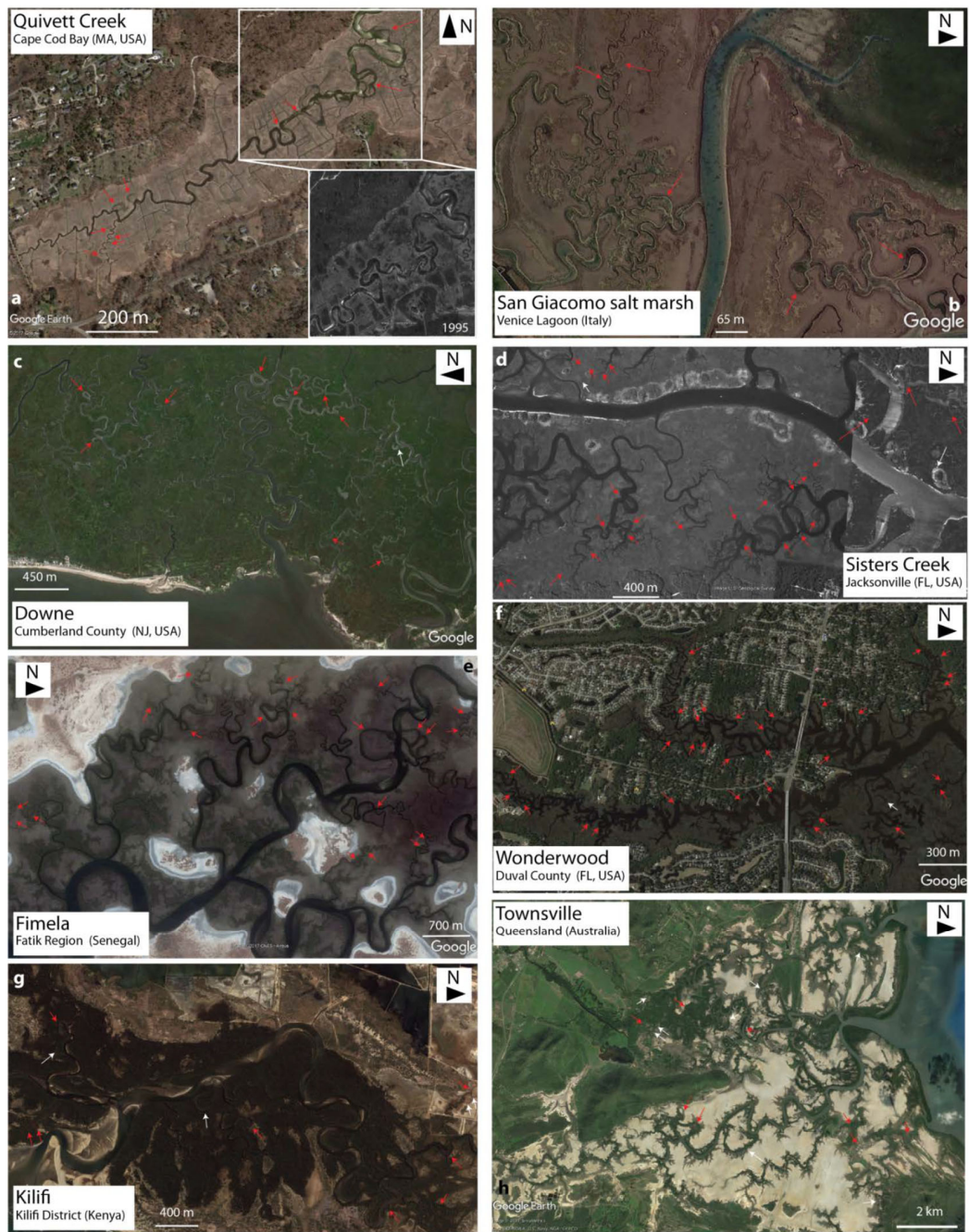


Figure S8. Identification of tidal meander cutoffs in different tidal settings worldwide. Red and white arrows indicate active and relic (i.e., unanalyzed) cutoffs, respectively.

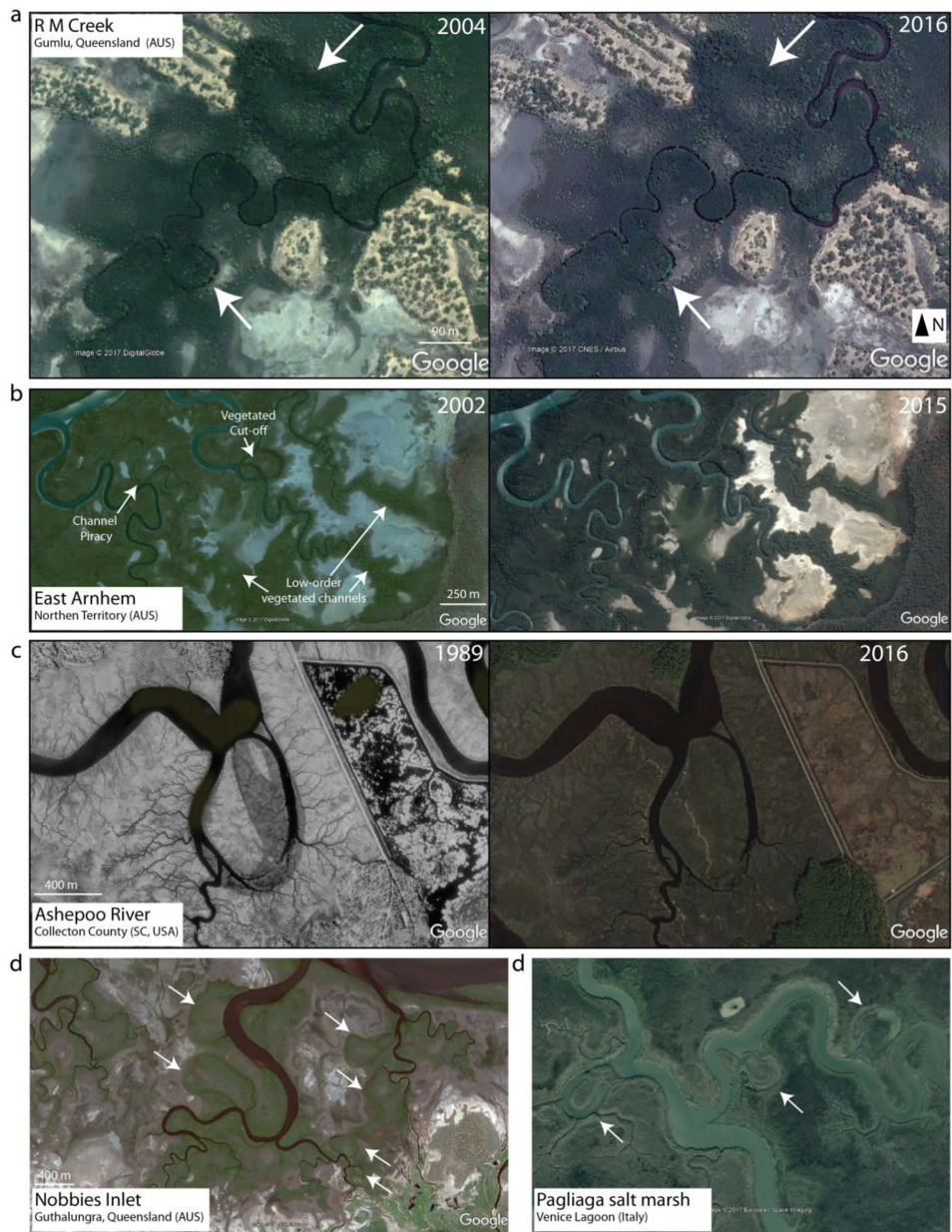


Figure S9. Examples of tidal meander cutoffs colonized by dense halophytic vegetation and/or incorporated into broader drainage network.

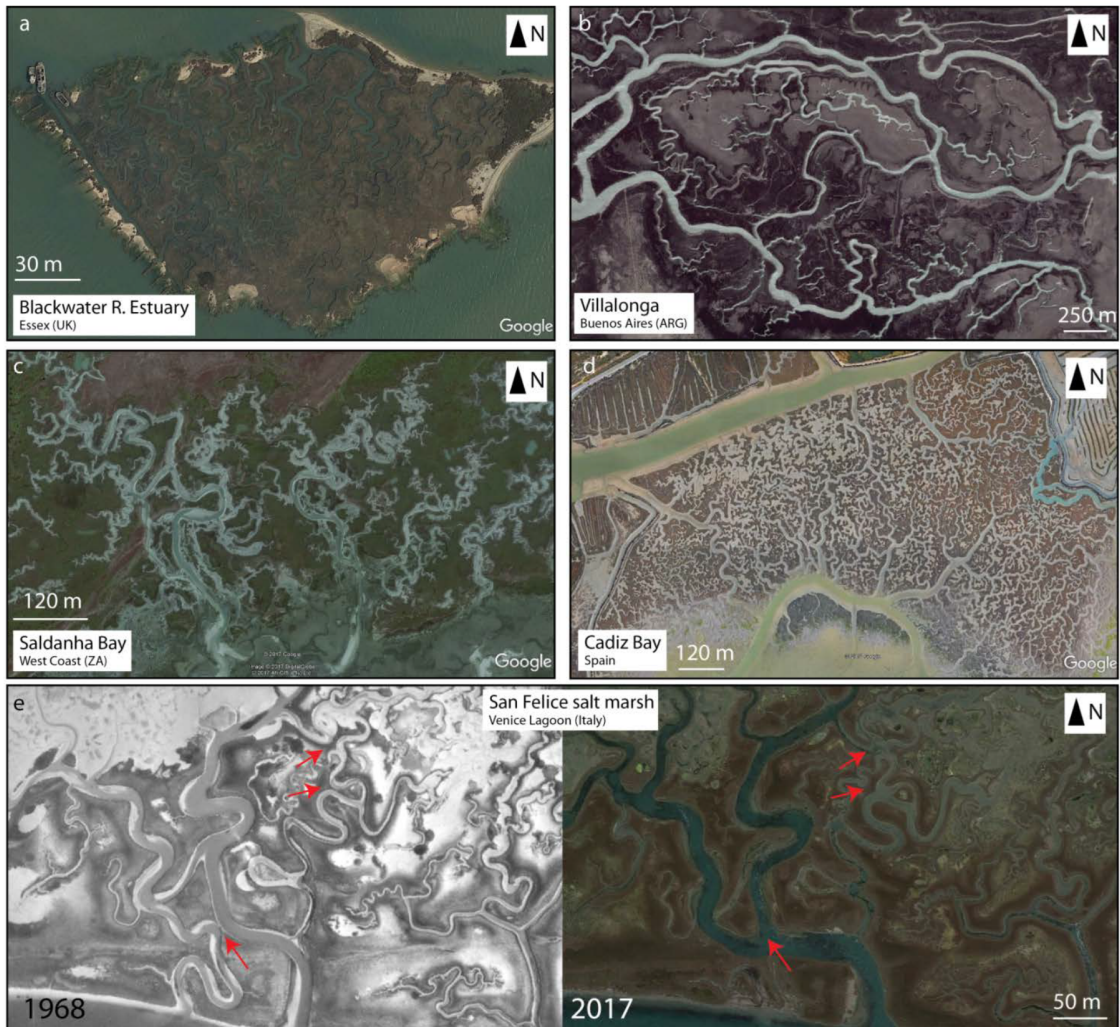


Figure S10. Examples of tidal wetlands characterized by high drainage densities that potentially limit freely meandering of tidal streams, as illustrated by the example reported in the bottom panel.

Table S1. KS test for tidal cutoffs and fluvial cutoffs ($\alpha = 0.05$)

Variable	Null Hypothesis H_0	Alternative Hyp. H_1	Rejected Null Hypothesis	p-value
R^*	$cdf_{tidal} = cdf_{fluvial}$	$cdf_{tidal} \neq cdf_{fluvial}$	Yes	$4.53e^{-9}$
	$cdf_{tidal} = cdf_{fluvial}$	$cdf_{tidal} > cdf_{fluvial}$	Yes	$2.27e^{-9}$
A^*	$cdf_{tidal} = cdf_{fluvial}$	$cdf_{tidal} \neq cdf_{fluvial}$	Yes	$3.17e^{-12}$
	$cdf_{tidal} = cdf_{fluvial}$	$cdf_{tidal} > cdf_{fluvial}$	Yes	$1.58e^{-12}$
ℓ^*	$cdf_{tidal} = cdf_{fluvial}$	$cdf_{tidal} \neq cdf_{fluvial}$	Yes	$8.56e^{-12}$
	$cdf_{tidal} = cdf_{fluvial}$	$cdf_{tidal} > cdf_{fluvial}$	Yes	$4.28e^{-12}$
χ	$cdf_{tidal} = cdf_{fluvial}$	$cdf_{tidal} \neq cdf_{fluvial}$	Yes	$6.28e^{-4}$
	$cdf_{tidal} = cdf_{fluvial}$	$cdf_{tidal} > cdf_{fluvial}$	Yes	$3.14e^{-4}$
\mathcal{A}	$cdf_{tidal} = cdf_{fluvial}$	$cdf_{tidal} \neq cdf_{fluvial}$	No	$4.90e^{-1}$
Φ_u	$cdf_{tidal} = cdf_{fluvial}$	$cdf_{tidal} \neq cdf_{fluvial}$	No	$4.22e^{-1}$

Table S2. KS test for microtidal cutoffs and mesotidal cutoffs ($\alpha = 0.05$)

Variable	Null Hypothesis H_0	Alternative Hyp. H_1	Rejected Null Hypothesis	p-value
R^*	$cdf_{micro} = cdf_{meso}$	$cdf_{micro} \neq cdf_{meso}$	Yes	$2.49e^{-7}$
	$cdf_{micro} = cdf_{meso}$	$cdf_{micro} > cdf_{meso}$	Yes	$1.25e^{-7}$
A^*	$cdf_{micro} = cdf_{meso}$	$cdf_{micro} \neq cdf_{meso}$	Yes	$1.42e^{-8}$
	$cdf_{micro} = cdf_{meso}$	$cdf_{micro} > cdf_{meso}$	Yes	$7.10e^{-9}$
ℓ^*	$cdf_{micro} = cdf_{meso}$	$cdf_{micro} \neq cdf_{meso}$	Yes	$3.62e^{-7}$
	$cdf_{micro} = cdf_{meso}$	$cdf_{micro} > cdf_{meso}$	Yes	$1.81e^{-7}$
χ	$cdf_{micro} = cdf_{meso}$	$cdf_{micro} \neq cdf_{meso}$	Yes	$1.62e^{-6}$
	$cdf_{micro} = cdf_{meso}$	$cdf_{micro} > cdf_{meso}$	Yes	$8.12e^{-7}$
\mathcal{A}	$cdf_{micro} = cdf_{meso}$	$cdf_{micro} \neq cdf_{meso}$	No	$3.60e^{-1}$
Φ_u	$cdf_{micro} = cdf_{meso}$	$cdf_{micro} \neq cdf_{meso}$	No	$6.80e^{-1}$
Φ_d	$cdf_{micro} = cdf_{meso}$	$cdf_{micro} \neq cdf_{meso}$	No	$3.00e^{-1}$

Table S3. KS test for microtidal cutoffs and macrotidal cutoffs ($\alpha = 0.05$)

Variable	Null Hypothesis H_0	Alternative Hyp. H_1	Rejected Null Hypothesis	p-value
R^*	$cdf_{micro} = cdf_{macro}$	$cdf_{micro} \neq cdf_{macro}$	No	$6.30e^{-1}$
A^*	$cdf_{micro} = cdf_{macro}$	$cdf_{micro} \neq cdf_{macro}$	No	$5.10e^{-1}$
ℓ^*	$cdf_{micro} = cdf_{macro}$	$cdf_{micro} \neq cdf_{macro}$	No	$3.90e^{-1}$
χ	$cdf_{micro} = cdf_{macro}$	$cdf_{micro} \neq cdf_{macro}$	No	$7.30e^{-1}$
\mathcal{A}	$cdf_{micro} = cdf_{macro}$	$cdf_{micro} \neq cdf_{macro}$	No	$8.30e^{-1}$
Φ_u	$cdf_{micro} = cdf_{macro}$	$cdf_{micro} \neq cdf_{macro}$	No	$3.00e^{-1}$
Φ_d	$cdf_{micro} = cdf_{macro}$	$cdf_{micro} \neq cdf_{macro}$	No	$6.70e^{-1}$

Table S4. KS test for mesotidal cutoffs and macrotidal cutoffs ($\alpha = 0.05$)

Variable	Null Hypothesis H_0	Alternative Hyp. H_1	Rejected Null Hypothesis	p-value
R^*	$cdf_{meso} = cdf_{macro}$	$cdf_{meso} \neq cdf_{macro}$	No	$1.00e^{-2}$
A^*	$cdf_{meso} = cdf_{macro}$	$cdf_{meso} \neq cdf_{macro}$	No	$1.90e^{-1}$
ℓ^*	$cdf_{meso} = cdf_{macro}$	$cdf_{meso} \neq cdf_{macro}$	No	$3.70e^{-1}$
χ	$cdf_{meso} = cdf_{macro}$	$cdf_{meso} \neq cdf_{macro}$	No	$2.70e^{-1}$
\mathcal{A}	$cdf_{meso} = cdf_{macro}$	$cdf_{meso} \neq cdf_{macro}$	No	$8.20e^{-1}$
Φ_u	$cdf_{meso} = cdf_{macro}$	$cdf_{meso} \neq cdf_{macro}$	No	$5.00e^{-2}$
Φ_d	$cdf_{meso} = cdf_{macro}$	$cdf_{meso} \neq cdf_{macro}$	No	$2.70e^{-1}$

Table S5. KS test for mangrove swamp cutoffs and salt marsh cutoffs ($\alpha = 0.05$)

Variable	Null Hypothesis H_0	Alternative Hyp. H_1	Rejected Null Hypothesis	p-value
R^*	$cdf_{mangrove} = cdf_{marsh}$	$cdf_{mangrove} \neq cdf_{marsh}$	Yes	$3.20e^{-9}$
	$cdf_{mangrove} = cdf_{marsh}$	$cdf_{mangrove} > cdf_{marsh}$	No	1.00
	$cdf_{mangrove} = cdf_{marsh}$	$cdf_{mangrove} < cdf_{marsh}$	Yes	$1.60e^{-9}$
A^*	$cdf_{mangrove} = cdf_{marsh}$	$cdf_{mangrove} \neq cdf_{marsh}$	Yes	$2.33e^{-15}$
	$cdf_{mangrove} = cdf_{marsh}$	$cdf_{mangrove} > cdf_{marsh}$	No	1.00
	$cdf_{mangrove} = cdf_{marsh}$	$cdf_{mangrove} < cdf_{marsh}$	Yes	$1.17e^{-15}$
ℓ^*	$cdf_{mangrove} = cdf_{marsh}$	$cdf_{mangrove} \neq cdf_{marsh}$	Yes	$9.66e^{-17}$
	$cdf_{mangrove} = cdf_{marsh}$	$cdf_{mangrove} > cdf_{marsh}$	No	1.00
	$cdf_{mangrove} = cdf_{marsh}$	$cdf_{mangrove} < cdf_{marsh}$	Yes	$4.83e^{-17}$
χ	$cdf_{mangrove} = cdf_{marsh}$	$cdf_{mangrove} \neq cdf_{marsh}$	Yes	$5.58e^{-6}$
	$cdf_{mangrove} = cdf_{marsh}$	$cdf_{mangrove} > cdf_{marsh}$	No	1.00
	$cdf_{mangrove} = cdf_{marsh}$	$cdf_{mangrove} < cdf_{marsh}$	Yes	$2.79e^{-6}$
\mathcal{A}	$cdf_{mangrove} = cdf_{marsh}$	$cdf_{mangrove} \neq cdf_{marsh}$	No	$2.00e^{-2}$
Φ_u	$cdf_{mangrove} = cdf_{marsh}$	$cdf_{mangrove} \neq cdf_{marsh}$	No	$2.10e^{-1}$
Φ_d	$cdf_{mangrove} = cdf_{marsh}$	$cdf_{mangrove} \neq cdf_{marsh}$	No	$6.70e^{-1}$

Table S6. KS test for mangrove swamp cutoffs and tidal flat cutoffs ($\alpha = 0.05$)

Variable	Null Hypothesis H_0	Alternative Hyp. H_1	Rejected Null Hypothesis	p-value
R^*	$cdf_{mangrove} = cdf_{flat}$	$cdf_{mangrove} \neq cdf_{flat}$	Yes	$7.00e^{-3}$
	$cdf_{mangrove} = cdf_{flat}$	$cdf_{mangrove} > cdf_{flat}$	Yes	$3.00e^{-3}$
A^*	$cdf_{mangrove} = cdf_{flat}$	$cdf_{mangrove} \neq cdf_{flat}$	No	$3.00e^{-2}$
ℓ^*	$cdf_{mangrove} = cdf_{flat}$	$cdf_{mangrove} \neq cdf_{flat}$	No	$4.00e^{-2}$
χ	$cdf_{mangrove} = cdf_{flat}$	$cdf_{mangrove} \neq cdf_{flat}$	No	$1.00e^{-1}$
\mathcal{A}	$cdf_{mangrove} = cdf_{flat}$	$cdf_{mangrove} \neq cdf_{flat}$	No	$2.50e^{-1}$
Φ_u	$cdf_{mangrove} = cdf_{flat}$	$cdf_{mangrove} \neq cdf_{flat}$	No	$8.70e^{-1}$
Φ_d	$cdf_{mangrove} = cdf_{flat}$	$cdf_{mangrove} \neq cdf_{flat}$	No	$9.90e^{-1}$

Table S7. KS test for salt marsh cutoffs and tidal flat cutoffs ($\alpha = 0.05$)

Variable	Null Hypothesis H_0	Alternative Hyp. H_1	Rejected Null Hypothesis	p-value
R^*	$cdf_{marsh} = cdf_{flat}$	$cdf_{marsh} \neq cdf_{flat}$	Yes	$1.84e^{-11}$
	$cdf_{marsh} = cdf_{flat}$	$cdf_{marsh} > cdf_{flat}$	Yes	$9.20e^{-12}$
A^*	$cdf_{marsh} = cdf_{flat}$	$cdf_{marsh} \neq cdf_{flat}$	Yes	$6.05e^{-13}$
	$cdf_{marsh} = cdf_{flat}$	$cdf_{marsh} > cdf_{flat}$	Yes	$3.02e^{-13}$
ρ^*	$cdf_{marsh} = cdf_{flat}$	$cdf_{marsh} \neq cdf_{flat}$	Yes	$2.77e^{-12}$
	$cdf_{marsh} = cdf_{flat}$	$cdf_{marsh} > cdf_{flat}$	Yes	$1.38e^{-12}$
χ	$cdf_{marsh} = cdf_{flat}$	$cdf_{marsh} \neq cdf_{flat}$	Yes	$2.69e^{-6}$
	$cdf_{marsh} = cdf_{flat}$	$cdf_{marsh} > cdf_{flat}$	Yes	$1.34e^{-6}$
\mathcal{A}	$cdf_{marsh} = cdf_{flat}$	$cdf_{marsh} \neq cdf_{flat}$	No	$6.00e^{-2}$
Φ_u	$cdf_{marsh} = cdf_{flat}$	$cdf_{marsh} \neq cdf_{flat}$	No	$7.00e^{-1}$
Φ_d	$cdf_{marsh} = cdf_{flat}$	$cdf_{marsh} \neq cdf_{flat}$	No	1.00

Table S8. KS test for bay cutoffs and lagoon cutoffs ($\alpha = 0.05$)

Variable	Null Hypothesis H_0	Alternative Hyp. H_1	Rejected Null Hypothesis	p-value
R^*	$cdf_{bay} = cdf_{lagoon}$	$cdf_{bay} \neq cdf_{lagoon}$	No	$2.62e^{-1}$
A^*	$cdf_{bay} = cdf_{lagoon}$	$cdf_{bay} \neq cdf_{lagoon}$	No	$1.50e^{-1}$
ρ^*	$cdf_{bay} = cdf_{lagoon}$	$cdf_{bay} \neq cdf_{lagoon}$	No	$1.58e^{-1}$
χ	$cdf_{bay} = cdf_{lagoon}$	$cdf_{bay} \neq cdf_{lagoon}$	No	$5.67e^{-2}$
\mathcal{A}	$cdf_{bay} = cdf_{lagoon}$	$cdf_{bay} \neq cdf_{lagoon}$	No	$1.28e^{-1}$
Φ_u	$cdf_{bay} = cdf_{lagoon}$	$cdf_{bay} \neq cdf_{lagoon}$	Yes	$3.09e^{-2}$
	$cdf_{bay} = cdf_{lagoon}$	$cdf_{bay} > cdf_{lagoon}$	Yes	$1.55e^{-2}$
Φ_d	$cdf_{bay} = cdf_{lagoon}$	$cdf_{bay} \neq cdf_{lagoon}$	No	$8.75e^{-1}$

Table S9. KS test for bay cutoffs and coast cutoffs ($\alpha = 0.05$)

Variable	Null Hypothesis H_0	Alternative Hyp. H_1	Rejected Null Hypothesis	p-value
R^*	$cdf_{bay} = cdf_{coast}$	$cdf_{bay} \neq cdf_{coast}$	Yes	$2.04e^{-8}$
	$cdf_{bay} = cdf_{coast}$	$cdf_{bay} > cdf_{coast}$	Yes	$1.02e^{-8}$
A^*	$cdf_{bay} = cdf_{coast}$	$cdf_{bay} \neq cdf_{coast}$	Yes	$3.93e^{-9}$
	$cdf_{bay} = cdf_{coast}$	$cdf_{bay} > cdf_{coast}$	Yes	$1.97e^{-9}$
ρ^*	$cdf_{bay} = cdf_{coast}$	$cdf_{bay} \neq cdf_{coast}$	Yes	$7.95e^{-10}$
	$cdf_{bay} = cdf_{coast}$	$cdf_{bay} > cdf_{coast}$	Yes	$3.98e^{-10}$
χ	$cdf_{bay} = cdf_{coast}$	$cdf_{bay} \neq cdf_{coast}$	Yes	$2.16e^{-5}$
	$cdf_{bay} = cdf_{coast}$	$cdf_{bay} > cdf_{coast}$	Yes	$1.08e^{-5}$
\mathcal{A}	$cdf_{bay} = cdf_{coast}$	$cdf_{bay} \neq cdf_{coast}$	Yes	$1.2e^{-3}$
	$cdf_{bay} = cdf_{coast}$	$cdf_{bay} > cdf_{coast}$	No	$9.84e^{-1}$
Φ_u	$cdf_{bay} = cdf_{coast}$	$cdf_{bay} < cdf_{coast}$	Yes	$5.85e^{-4}$
	$cdf_{bay} = cdf_{coast}$	$cdf_{bay} \neq cdf_{coast}$	No	$9.89e^{-2}$
Φ_d	$cdf_{bay} = cdf_{coast}$	$cdf_{bay} \neq cdf_{coast}$	Yes	$3.05e^{-2}$
	$cdf_{bay} = cdf_{coast}$	$cdf_{bay} > cdf_{coast}$	Yes	$1.53e^{-2}$

Table S10. KS test for bay cutoffs and estuary cutoffs ($\alpha = 0.05$)

Variable	Null Hypothesis H_0	Alternative Hyp. H_1	Rejected Null Hypothesis	p-value
R^*	$cdf_{bay} = cdf_{estuary}$	$cdf_{bay} \neq cdf_{estuary}$	Yes	$1.70e^{-2}$
	$cdf_{bay} = cdf_{estuary}$	$cdf_{bay} > cdf_{estuary}$	Yes	$8.5e^{-3}$
A^*	$cdf_{bay} = cdf_{estuary}$	$cdf_{bay} \neq cdf_{estuary}$	Yes	$3.71e^{-2}$
	$cdf_{bay} = cdf_{estuary}$	$cdf_{bay} > cdf_{estuary}$	Yes	$1.85e^{-2}$
ρ^*	$cdf_{bay} = cdf_{estuary}$	$cdf_{bay} \neq cdf_{estuary}$	No	$6.37e^{-2}$
χ	$cdf_{bay} = cdf_{estuary}$	$cdf_{bay} \neq cdf_{estuary}$	Yes	$6.39e^{-4}$
	$cdf_{bay} = cdf_{estuary}$	$cdf_{bay} > cdf_{estuary}$	Yes	$3.20e^{-4}$
\mathcal{A}	$cdf_{bay} = cdf_{estuary}$	$cdf_{bay} \neq cdf_{estuary}$	Yes	$1.50e^{-3}$
	$cdf_{bay} = cdf_{estuary}$	$cdf_{bay} > cdf_{estuary}$	No	$8.21e^{-1}$
Φ_u	$cdf_{bay} = cdf_{estuary}$	$cdf_{bay} < cdf_{estuary}$	Yes	$7.55e^{-4}$
	$cdf_{bay} = cdf_{estuary}$	$cdf_{bay} \neq cdf_{estuary}$	No	$7.27e^{-2}$
Φ_d	$cdf_{bay} = cdf_{estuary}$	$cdf_{bay} \neq cdf_{estuary}$	No	$5.74e^{-1}$

Table S11. KS test for lagoon cutoffs and coast cutoffs ($\alpha = 0.05$)

Variable	Null Hypothesis H_0	Alternative Hyp. H_1	Rejected Null Hypothesis	p-value
R^*	$cdf_{lagoon} = cdf_{coast}$	$cdf_{lagoon} \neq cdf_{coast}$	Yes	$6.08e^{-8}$
	$cdf_{lagoon} = cdf_{coast}$	$cdf_{lagoon} > cdf_{coast}$	Yes	$3.04e^{-8}$
A^*	$cdf_{lagoon} = cdf_{coast}$	$cdf_{lagoon} \neq cdf_{coast}$	Yes	$4.95e^{-11}$
	$cdf_{lagoon} = cdf_{coast}$	$cdf_{lagoon} > cdf_{coast}$	Yes	$2.47e^{-11}$
ρ^*	$cdf_{lagoon} = cdf_{coast}$	$cdf_{lagoon} \neq cdf_{coast}$	Yes	$5.48e^{-12}$
	$cdf_{lagoon} = cdf_{coast}$	$cdf_{lagoon} > cdf_{coast}$	Yes	$2.74e^{-12}$
χ	$cdf_{lagoon} = cdf_{coast}$	$cdf_{lagoon} \neq cdf_{coast}$	Yes	$1.39e^{-2}$
	$cdf_{lagoon} = cdf_{coast}$	$cdf_{lagoon} > cdf_{coast}$	Yes	$6.90e^{-3}$
\mathcal{A}	$cdf_{lagoon} = cdf_{coast}$	$cdf_{lagoon} \neq cdf_{coast}$	No	$5.76e^{-2}$
Φ_u	$cdf_{lagoon} = cdf_{coast}$	$cdf_{lagoon} \neq cdf_{coast}$	No	$9.83e^{-1}$
Φ_d	$cdf_{lagoon} = cdf_{coast}$	$cdf_{lagoon} \neq cdf_{coast}$	No	$1.83e^{-1}$

Table S12. KS test for lagoon cutoffs and estuary cutoffs ($\alpha = 0.05$)

Variable	Null Hypothesis H_0	Alternative Hyp. H_1	Rejected Null Hypothesis	p-value
R^*	$cdf_{lagoon} = cdf_{estuary}$	$cdf_{lagoon} \neq cdf_{estuary}$	No	$5.65e^{-2}$
A^*	$cdf_{lagoon} = cdf_{estuary}$	$cdf_{lagoon} \neq cdf_{estuary}$	Yes	$4.9e^{-3}$
	$cdf_{lagoon} = cdf_{estuary}$	$cdf_{lagoon} > cdf_{estuary}$	Yes	$2.5e^{-3}$
ρ^*	$cdf_{lagoon} = cdf_{estuary}$	$cdf_{lagoon} \neq cdf_{estuary}$	Yes	$2.17e^{-2}$
	$cdf_{lagoon} = cdf_{estuary}$	$cdf_{lagoon} > cdf_{estuary}$	Yes	$1.09e^{-2}$
χ	$cdf_{lagoon} = cdf_{estuary}$	$cdf_{lagoon} \neq cdf_{estuary}$	Yes	$1.58e^{-2}$
	$cdf_{lagoon} = cdf_{estuary}$	$cdf_{lagoon} > cdf_{estuary}$	Yes	$7.9e^{-3}$
\mathcal{A}	$cdf_{lagoon} = cdf_{estuary}$	$cdf_{lagoon} \neq cdf_{estuary}$	No	$6.06e^{-2}$
Φ_u	$cdf_{lagoon} = cdf_{estuary}$	$cdf_{lagoon} \neq cdf_{estuary}$	No	$7.48e^{-1}$
Φ_d	$cdf_{lagoon} = cdf_{estuary}$	$cdf_{lagoon} \neq cdf_{estuary}$	No	$5.96e^{-1}$

Table S13. KS test for coast cutoffs and estuary cutoffs ($\alpha = 0.05$)

Variable	Null Hypothesis H_0	Alternative Hyp. H_1	Rejected Null Hypothesis	p-value
R^*	$cdf_{coast} = cdf_{estuary}$	$cdf_{coast} \neq cdf_{estuary}$	Yes	$9.88e^{-5}$
	$cdf_{coast} = cdf_{estuary}$	$cdf_{coast} > cdf_{estuary}$	No	$9.65e^{-1}$
	$cdf_{coast} = cdf_{estuary}$	$cdf_{coast} < cdf_{estuary}$	Yes	$4.94e^{-5}$
A^*	$cdf_{coast} = cdf_{estuary}$	$cdf_{coast} \neq cdf_{estuary}$	Yes	$8.66e^{-4}$
	$cdf_{coast} = cdf_{estuary}$	$cdf_{coast} > cdf_{estuary}$	No	$9.65e^{-1}$
	$cdf_{coast} = cdf_{estuary}$	$cdf_{coast} < cdf_{estuary}$	Yes	$4.33e^{-4}$
ℓ^*	$cdf_{coast} = cdf_{estuary}$	$cdf_{coast} \neq cdf_{estuary}$	Yes	$3.26e^{-4}$
	$cdf_{coast} = cdf_{estuary}$	$cdf_{coast} > cdf_{estuary}$	No	$9.91e^{-1}$
	$cdf_{coast} = cdf_{estuary}$	$cdf_{coast} < cdf_{estuary}$	Yes	$1.63e^{-4}$
χ	$cdf_{coast} = cdf_{estuary}$	$cdf_{coast} \neq cdf_{estuary}$	No	$1.00e^{-1}$
\mathcal{A}	$cdf_{coast} = cdf_{estuary}$	$cdf_{coast} \neq cdf_{estuary}$	No	$2.43e^{-1}$
Φ_u	$cdf_{coast} = cdf_{estuary}$	$cdf_{coast} \neq cdf_{estuary}$	No	$7.76e^{-1}$
Φ_d	$cdf_{coast} = cdf_{estuary}$	$cdf_{coast} \neq cdf_{estuary}$	Yes	$3.39e^{-2}$
	$cdf_{coast} = cdf_{estuary}$	$cdf_{coast} > cdf_{estuary}$	No	$6.82e^{-1}$
	$cdf_{coast} = cdf_{estuary}$	$cdf_{coast} < cdf_{estuary}$	Yes	$1.69e^{-2}$